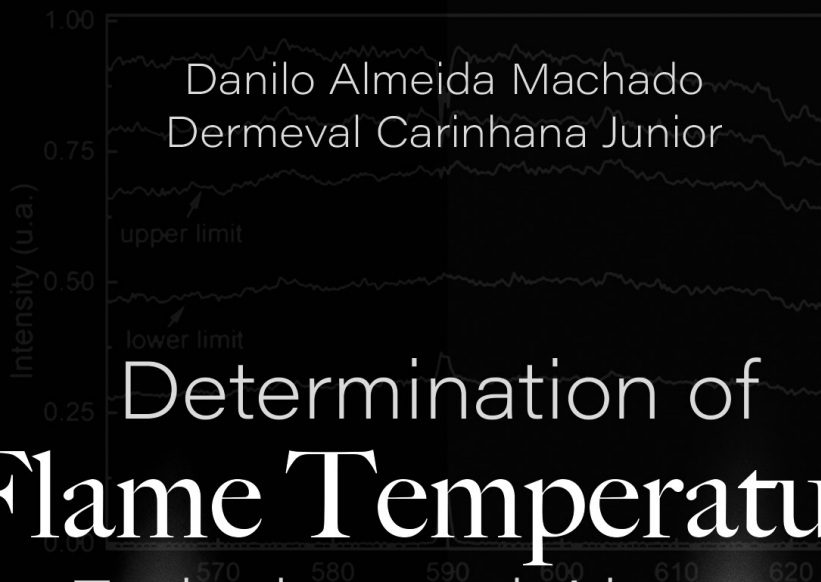


Danilo Almeida Machado
Dermeval Carinhana Junior

Determination of Flame Temperature by Emission and Absorption Spectroscopy





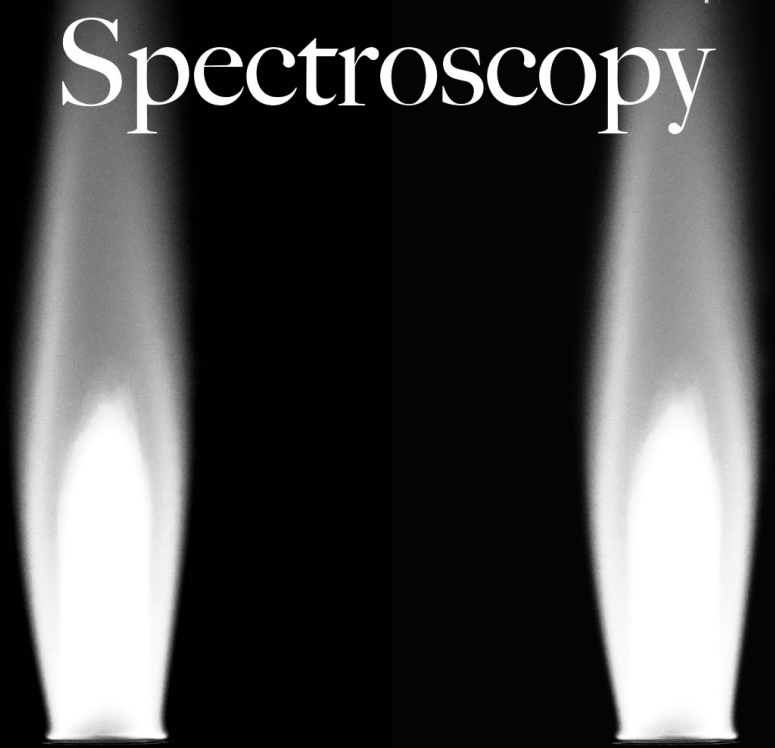
Danilo Almeida Machado
Dermeval Carinhana Junior

Determination of

Flame Temperature

by Emission and Absorption

Spectroscopy



Chief editor

Profª Drª Antonella Carvalho de Oliveira

Executive editor

Natalia Oliveira

Editorial assistant

Flávia Roberta Barão

Librarian

Janaina Ramos

Graphic project

Ellen Andressa Kubisty

Luiza Alves Batista

Nataly Evilin Gayde

Thamires Camili Gayde

Cover pictures

iStock

Art edition

Luiza Alves Batista

2024 by Atena Editora

Copyright © Atena Editora

Copyright of the text © 2024 The authors

Copyright of the edition © 2024 Atena Editora

Rights for this edition granted to Atena Editora by the authors.

Open access publication by Atena Editora



All content in this book is licensed under a Creative Commons Attribution License. Attribution-Non-Commercial-NonDerivatives 4.0 International (CC BY-NC-ND 4.0).

The content of the text and their data in their form, correctness and reliability are the sole responsibility of the authors, and they do not necessarily represent the official position of Atena Editora. It is allowed to download the work and share it as long as credits are given to the authors, but without the possibility of altering it in any way or using it for commercial purposes.

All manuscripts were previously submitted to blind evaluation by peers, members of the Editorial Board of this Publisher, having been approved for publication based on criteria of academic neutrality and impartiality.

Atena Editora is committed to ensuring editorial integrity at all stages of the publication process, avoiding plagiarism, fraudulent data or results and preventing financial interests from compromising the publication's ethical standards. Suspected scientific misconduct situations will be investigated to the highest standard of academic and ethical rigor.

Editorial Board**Exact and earth sciences and engineering**

Prof. Dr. Adélio Alcino Sampaio Castro Machado – Universidade do Porto

Profª Drª Alana Maria Cerqueira de Oliveira – Instituto Federal do Acre

Profª Drª Ana Grasielle Dionísio Corrêa – Universidade Presbiteriana Mackenzie

Profª Drª Ana Paula Florêncio Aires – Universidade de Trás-os-Montes e Alto Douro

Prof. Dr. Carlos Eduardo Sanches de Andrade – Universidade Federal de Goiás

Profª Drª Carmen Lúcia Voigt – Universidade Norte do Paraná

Prof. Dr. Cleiseano Emanuel da Silva Paniagua – Colégio Militar Dr. José Aluisio da Silva Luz / Colégio Santa Cruz de Araguaína/TO

Profª Drª Cristina Aledi Felseburgh – Universidade Federal do Oeste do Pará

Prof. Dr. Diogo Peixoto Cordova – Universidade Federal do Pampa, Campus Caçapava do Sul

Prof. Dr. Douglas Gonçalves da Silva – Universidade Estadual do Sudoeste da Bahia

Prof. Dr. Eloi Rufato Junior – Universidade Tecnológica Federal do Paraná

Profª Drª Érica de Melo Azevedo – Instituto Federal do Rio de Janeiro

Prof. Dr. Fabrício Menezes Ramos – Instituto Federal do Pará

Prof. Dr. Fabrício Moraes de Almeida – Universidade Federal de Rondônia

Profª Drª Glécilla Colombelli de Souza Nunes – Universidade Estadual de Maringá

Prof. Dr. Hauster Maximiler Campos de Paula – Universidade Federal de Viçosa

Profª Drª Iara Margolis Ribeiro – Universidade Federal de Pernambuco

Profª Drª Jéssica Barbosa da Silva do Nascimento – Universidade Estadual de Santa Cruz

Profª Drª Jéssica Verger Nardeli – Universidade Estadual Paulista Júlio de Mesquita Filho

Prof. Dr. Juliano Bitencourt Campos – Universidade do Extremo Sul Catarinense

Prof. Dr. Juliano Carlo Rufino de Freitas – Universidade Federal de Campina Grande

Prof. Dr. Leonardo França da Silva – Universidade Federal de Viçosa

Profª Drª Luciana do Nascimento Mendes – Instituto Federal de Educação, Ciência e Tecnologia do Rio Grande do Norte

Prof. Dr. Marcelo Marques – Universidade Estadual de Maringá

Prof. Dr. Marco Aurélio Kistemann Junior – Universidade Federal de Juiz de Fora

Prof. Dr. Marcos Vinicius Winckler Caldeira – Universidade Federal do Espírito Santo

Profª Drª Maria Iaponeide Fernandes Macêdo – Universidade do Estado do Rio de Janeiro

Profª Drª Maria José de Holanda Leite – Universidade Federal de Alagoas

Profª Drª Mariana Natale Fiorelli Fabiche – Universidade Estadual de Maringá

Prof. Dr. Miguel Adriano Inácio – Instituto Nacional de Pesquisas Espaciais

Prof. Dr. Milson dos Santos Barbosa – Universidade Tiradentes

Profª Drª Natiéli Piovesan – Instituto Federal do Rio Grande do Norte

Profª Drª Neiva Maria de Almeida – Universidade Federal da Paraíba

Prof. Dr. Nilzo Ivo Ladwig – Universidade do Extremo Sul Catarinense

Profª Drª Priscila Natasha Kinas – Universidade do Estado de Santa Catarina

Profª Drª Priscila Tessmer Scaglioni – Universidade Federal de Pelotas

Prof. Dr. Rafael Pacheco dos Santos – Universidade do Estado de Santa Catarina

Prof. Dr. Ramiro Picoli Nippes – Universidade Estadual de Maringá

Profª Drª Regina Célia da Silva Barros Allil – Universidade Federal do Rio de Janeiro

Prof. Dr. Sidney Gonçalo de Lima – Universidade Federal do Piauí

Prof. Dr. Takeshy Tachizawa – Faculdade de Campo Limpo Paulista

Determination of flame temperature by emission and absorption spectroscopy

Diagramming: Nataly Gayde
Correction: Maiara Ferreira
Indexing: Amanda Kelly da Costa Veiga
Review: The authors
Authors: Danilo Almeida Machado
Dermeval Carinhana Junior

International Cataloging-in-Publication Data (CIP)	
M149	<p>Machado, Danilo Almeida Determination of flame temperature by emission and absorption spectroscopy / Danilo Almeida Machado, Dermeval Carinhana Junior. – Ponta Grossa - PR: Atena, 2024.</p> <p>Format: PDF System requirements: Adobe Acrobat Reader Access mode: World Wide Web Includes bibliography ISBN 978-65-258-2702-5 DOI: https://doi.org/10.22533/at.ed.025241608</p> <p>1. Combustion. 2. Temperature. 3. Liquefied Petroleum Gas (LPG). I. Machado, Danilo Almeida. II. Carinhana Junior, Dermeval. III. Title.</p> <p style="text-align: right;">CDD 541.36</p>
Prepared by Librarian Janaina Ramos – CRB-8/9166	

Atena Editora
Ponta Grossa – Paraná – Brasil
Telephone: +55 (42) 3323-5493
www.atenaeditora.com.br
contato@atenaeditora.com.br

AUTHORS' DECLARATION

The authors of this work: 1. Attest that they do not have any commercial interest that constitutes a conflict of interest in relation to the published scientific article; 2. They declare that they actively participated in the construction of their manuscripts, preferably in: a) Study design, and/or data acquisition, and/or data analysis and interpretation; b) Elaboration of the article or revision in order to make the material intellectually relevant; c) Final approval of the manuscript for submission; 3. They certify that published scientific articles are completely free from fraudulent data and/or results; 4. Confirm correct citation and reference of all data and interpretations of data from other research; 5. They acknowledge having informed all sources of funding received for carrying out the research; 6. Authorize the publication of the work, which includes the catalog records, ISBN (Internacional Standard Serial Number), D.O.I. (Digital Object Identifier) and other indexes, visual design and cover creation, interior layout, as well as the release and dissemination according to Atena Editora's criteria.

PUBLISHER'S DECLARATION

Atena Editora declares, for all legal purposes, that: 1. This publication constitutes only a temporary transfer of copyright, right to publication, and does not constitute joint and several liability in the creation of published manuscripts, under the terms provided for in the Law on Rights copyright (Law 9610/98), in art. 184 of the Penal Code and in art. 927 of the Civil Code; 2. Authorizes and encourages authors to sign contracts with institutional repositories, with the exclusive purpose of disseminating the work, provided that with due acknowledgment of authorship and editing and without any commercial purpose; 3. All e-books are open access, so it does not sell them on its website, partner sites, e-commerce platforms, or any other virtual or physical means, therefore, it is exempt from copyright transfers to authors; 4. All members of the editorial board are PhDs and linked to public higher education institutions, as recommended by CAPES for obtaining the Qualis book; 5. It does not transfer, commercialize or authorize the use of the authors' names and e-mails, as well as any other data from them, for any purpose other than the scope of dissemination of this work.

This book is dedicated to all students and professionals in the field of combustion. It is written as a basic text, designed to provide foundational knowledge and practical insights into the measurement of flame temperature using a low-cost technique.

My hope is that this book serves as a valuable resource, inspiring curiosity, enhancing understanding, and fostering innovation within the combustion community. Whether you are just beginning your journey or are an experienced professional, may this book contribute to your continued growth and success in this fascinating and essential field.

First and foremost, I dedicate this book to God, whose guidance and blessings have been my constant source of strength and inspiration.

I also want to express my deep gratitude to the friends I have made over the past 15 years during my experiences in the field of combustion at the São Paulo State University (UNESP), the Institute of Advanced Studies (IEAv), the Aeronautics Institute of Technology (ITA), the National Institute for Space Research (INPE), and the University of São Paulo (USP). Your support, camaraderie, and shared knowledge have been invaluable. A special thank you to Prof. Dermeval, who taught me the fundamentals of good experimental work and sparked my interest in the laboratory.

To my beloved family, I dedicate this work with heartfelt thanks. To my wife, Gabriela, your unwavering love and encouragement have been my anchor. To my son, Antonio, your curiosity and joy remind me daily of the importance of pursuing one's passions. To my brother, Jose Mario, your constant support has been a pillar of strength, and in memory of my mother Renisia.

This book is a reflection of the collective wisdom, support, and love I have received from each of you. Thank you for being a part of this journey.

This book, "Determination of Flame Temperature by Emission and Absorption Spectroscopy," aims to provide a comprehensive guide for students and professionals in the field of combustion. Over the years, the importance of accurate temperature measurement in combustion processes has become increasingly evident. This book is intended to serve as a foundational text, offering both theoretical insights and practical methodologies for measuring flame temperature using cost-effective techniques.

The primary focus of this book is on the use of emission and absorption spectroscopy to determine flame temperatures. These optical measurement techniques are non-intrusive and allow for precise temperature determination, essential for optimizing combustion processes and reducing pollutant emissions. By leveraging these techniques, researchers and engineers can develop more efficient combustion systems and advance the understanding of high-temperature combustion processes.

The content is structured to guide the reader through the theoretical foundations of spectroscopy, the principles of combustion, and the practical aspects of implementing these measurement techniques. It begins with an introduction to the significance of optical measurement in combustion, followed by detailed discussions on the underlying physical principles, including blackbody radiation, the laws of radiation, and the mechanisms of absorption and emission.

Subsequent chapters delve into the specific methodologies used in emission and absorption spectroscopy, providing step-by-step procedures for obtaining and analyzing spectral data. The book also compares different techniques, such as the Boltzmann plot method and the sodium line reversal technique, offering insights into their respective advantages and applications.

Throughout the book, real-world examples and experimental results are presented to illustrate the practical applications of these techniques. The aim is to equip readers with the knowledge and skills necessary to perform accurate flame temperature measurements and to apply these techniques in various combustion research and industrial scenarios.

By the end of this book, readers will have a thorough understanding of the principles and practices of emission and absorption spectroscopy in combustion diagnostics. It is my hope that this book will serve as a valuable resource, inspiring further research and innovation in the field of combustion, and contributing to the development of cleaner, more efficient combustion technologies.

In a combustion process involving fossil fuels, there is the formation of species Chemiluminescent, especially CH^* , C_2^* and OH^* , whose spontaneous emission can be used as a diagnostic tool. In the present work, mapping and determination of the rotational temperature of the species CH^* produced in flames on a burner fueled by Liquefied Petroleum Gas (LPG) was carried out. This study is part of a project involving the characterization of supersonic combustion in "scramjets" engines, whose study has been conducted in the hypersonic shock tunnel IEAv laboratories. The technique used was the natural emission spectroscopy, which has as main advantage of being non-intrusive. The rotational temperature determination was made using the Boltzmann method, whose principle is to relate the emission intensity of the species to the temperature by means of spectroscopic constants established. The temperature values were determined from the analysis of electronic bands AX and BX of the radical CH^* . In order to confirm the results of flame temperatures obtained by the natural emission technique, was also used the technique of line reversal sodium. The results of both techniques showed that the temperature of the flames investigated is about 2500K a 2700K.

KEYWORDS: Combustion; Diagnostics, Temperature; Liquefied Petroleum Gas (LPG).

1. INTRODUCTION.....	1
2. THEORETICAL FOUNDATION	3
2.1 Early Spectroscopic Studies	3
2.2 Surface Properties of a Body	3
2.3 Black Body Radiation	5
2.4 Laws of Radiation.....	6
2.5 Basic Concepts: Absorption and Emission Processes.....	8
2.6 Emission Energy	11
2.7 Combustion.....	15
2.8 Flame Temperature	24
2.9 Temperature Determination by Natural Emission Technique	25
2.10 Equivalence Ratio.....	26
2.11 Temperature Determination by the Sodium Line Reversal Technique.....	26
3. METHODOLOGY.....	28
3.1 Natural Emission Spectroscopy.....	28
3.2 Sodium Line Reversal	31
4. RESULTS AND DISCUSSION	32
4.1 - Radical Mapping	32
4.2 Temperatures Calculated Using the Natural Emission Technique.....	34
4.3 Temperatures Calculated Using the Sodium Line Reversal Technique.....	36
CONCLUSION.....	38
BIBLIOGRAPHY	39
ABOUT THE AUTHOR	41

INTRODUCTION

The importance of optical measurement techniques in combustion systems lies in their ability to provide non-intrusive data. Optical measurement techniques have emerged as an indispensable tool in various research areas and industrial applications, particularly in the analysis of combustion processes. These techniques offer several advantages over traditional temperature measurement methods, such as thermocouples, which are limited to temperatures below 2000 K and are intrusive by nature (MILES, 2015). Optical techniques, on the other hand, are non-intrusive and allow measurements at much higher temperatures, essential for monitoring high-temperature combustion processes.

Temperature is a critical variable in combustion processes, directly influencing combustion efficiency and pollutant formation. Accurate temperature measurement in flames enables more precise control of combustion processes, facilitating the development of more efficient systems with lower pollutant emissions and the advancement of new fuels (DIAS et al., 2023; MOTA et al., 2024). Studies have shown that fuels such as liquefied petroleum gas (LPG) burn more cleanly compared to gasoline and diesel, with lower emissions of CO, CO₂, NO, and particulates (KIM et al., 2024; SIMSEK; USLU, 2020)

The technique of temperature determination by spectroscopy using Boltzmann plots is based on observing the intensities of spectral lines emitted by molecules in excited states within a flame. Essentially, when a molecule in a high-energy state returns to a lower energy state, it emits light at specific wavelengths. The intensity of this light, which can be measured with a spectrometer, is related to the flame temperature, as the distribution of molecules across different energy states follows Boltzmann's distribution law. By recording these intensities and analyzing how they vary with the energy levels of the excited states, it is possible to determine the flame temperature accurately (BORKOWSKA-BURNECKA et al., 2004; CARINHANA JR. et al., 2008).

To apply this technique, emission spectra are obtained and analyzed using a low-cost, high-speed optical spectrometer. The data are then represented graphically, showing the relationship between the emitted light intensity and the energy of the excited states of the molecules. This graph, known as a Boltzmann plot, exhibits a linear distribution, the slope of which is used to calculate the temperature.

The sodium line reversal (SLR) technique, meanwhile, has been used for over a century in various fields. The temperature of a flame can be determined by balancing the emission and absorption coefficients in the same wavelength, according to Kirchhoff's law. This approach was first adopted by Kurlbaum in 1902 to determine flame temperature using carbon particles. In 1903, Fery used a sodium resonant line to determine temperatures of flames (GAYDON; WOLFHARD, 1952). The SLR method, based on Kirchhoff's law, has been used for over a century to determine the temperature in various fields, including plasmas (KARABOURNIOTIS, 2007), shock tunnels (HURLE; RUSSO, 1965), Kelvin-

Helmholtz instabilities (FUJISAWA et al., 2014), pyrolysis reactions (DRAKON et al., 2018), the study of soot in rich flames (Pejpichestakul et al., 2019), magnetohydrodynamic (MHD) generator, in conjunction with oxy-fuel combustion (BEDICK et al., 2020) and SCRAMJET engines (OSGERBY; SMITHSON; WAGNER, 1970). The simplicity of the SLR technique allows its application in field tests, such as firing solid propellant rocket engines (YANG et al., 2001), or in modified and more complex versions that can be employed for determining the temperature of hybrid propulsion rocket plumes (SIMURDA et al., 2020).

The objective of this book is to demonstrate, from both theoretical and experimental perspectives, two optical diagnostic techniques for measuring flame temperatures that are low-cost and easy to operate. These techniques, known as the determination of temperature by natural emission spectra of the flame and the sodium line reversal method, will be used to determine the temperatures of liquefied petroleum gas flames at various equivalence ratios. Through detailed explanations and practical examples, this book aims to provide readers with a comprehensive understanding of these methods, making them accessible for use in a variety of combustion research and industrial applications.

This book is the result of Danilo Almeida Machado's undergraduate work at UNESP, supervised by Prof. Dermeval Carinhana Junior.

THEORETICAL FOUNDATION

2.1 EARLY SPECTROSCOPIC STUDIES

The earliest spectroscopic studies were based on the analysis of sunlight. Joseph Fraunhofer was one of the pioneers in studying sunlight using an optical component later known as a diffraction grating, which contained a series of grooves capable of diffracting sunlight. Fraunhofer discovered that, when passing through the diffraction grating, sunlight experienced a deviation in its trajectory, with the intensity directly proportional to its wavelength. The projection of the refracted light onto a screen resulted in a continuous spectrum of sunlight, arranged similarly to the formation of a rainbow on rainy days. However, upon closely observing the diffracted sunlight, Fraunhofer noted hundreds of discrete dark lines, i.e., with well-defined spectral positions, superimposed on the continuous spectrum. Besides the Sun, other light sources were used by the pioneers of spectroscopic techniques. By studying the light emitted by incandescent objects, Fraunhofer observed discrete spectra instead of the continuous spectrum like that of the Sun, with lines corresponding to the spectral positions of the dark lines present in the solar spectrum. However, it was two other Germans, Robert W. Bunsen and Gustav R. Kirchhoff, who discovered the origin of these lines. Working with the introduction of dissolved salts, such as sodium chloride, into gas flames, Bunsen and Kirchhoff observed the emission of light at wavelengths characteristic of each chemical species. The recording of these lines became known as the emission spectrum. In the case of sodium, the strongest emission was observed in the region of 589 nm, corresponding to a yellow coloration. They concluded that the dark lines originated from the absorption of sunlight by certain chemical elements present in the gaseous layer surrounding the Earth. Thus, the absorption spectrum of the Earth's atmosphere was discovered (FILGUEIRAS, 1996; LAGALANTE, 2004).

2.2 SURFACE PROPERTIES OF A BODY

The term radiation refers to the continuous emission of energy from the surface of any body, where the energy is termed radiant and is transported by electromagnetic waves traveling in a vacuum at a speed of 3×10^8 m/s. Radio waves, infrared radiation, visible light, ultraviolet light, X-rays, and gamma rays constitute the different regions of the electromagnetic spectrum.

A body surface is constantly exposed to radiant energy, both from the interior and the exterior, with the external energy coming from objects surrounding the body. Figure 1 shows the incidence of a light beam, where radiant energy hits the surface, part of it is reflected, and the other part is transmitted (RUARK, 1960).

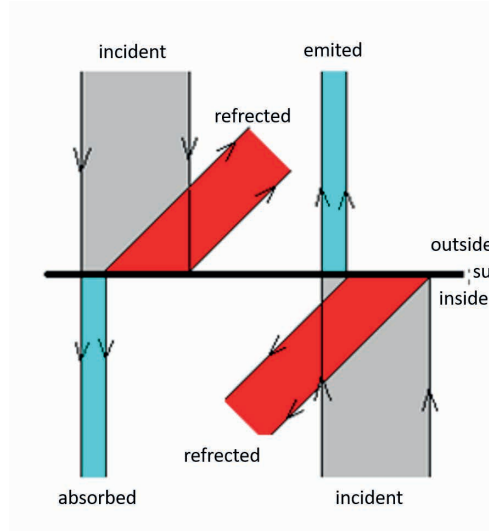


Figure 1. Radiation incident on the surface of a body.

The figure 1 illustrates the processes of radiation interaction with the surface of a body, highlighting the phenomena of incidence, reflection, absorption, and emission. Incident light rays from the exterior encounter the surface of the body, where part of this radiation is reflected back to the exterior while another part is absorbed by the material. The absorbed energy is then re-emitted, manifesting as emitted radiation that can cross the surface of the body. This emission process is evidenced by the emitted ray propagating outward from the body. Internally, incident rays can be reflected within the material or contribute to external emission. Thus, the figure represents the dynamics of energy transfer at the interface between the interior and exterior of the body, demonstrating the interdependence between the phenomena of absorption, emission, and reflection at the material surface.

It is considered the radiant energy that is incident from the exterior onto the surface of the body. If the surface is smooth and polished, like that of a mirror, most of the incident energy is reflected, while the rest passes through the surface of the body and is absorbed by its atoms or molecules. If (r) is the proportion of radiant energy that is reflected, and (a) is the proportion that is absorbed, it must hold that $r + a = 1$.

The same proportion (r) of the radiant energy incident from the interior is reflected inward, and the proportion ($a = 1 - r$) is transmitted outward, and is therefore called the radiant energy emitted by the surface.

Figures 1 and 2 show the behaviors of the surface of a body that reflects a small part of the incident energy. The widths of the different bands correspond to relative amounts of incident, reflected, and transmitted radiant energy through the surface (RUARK, 1960).

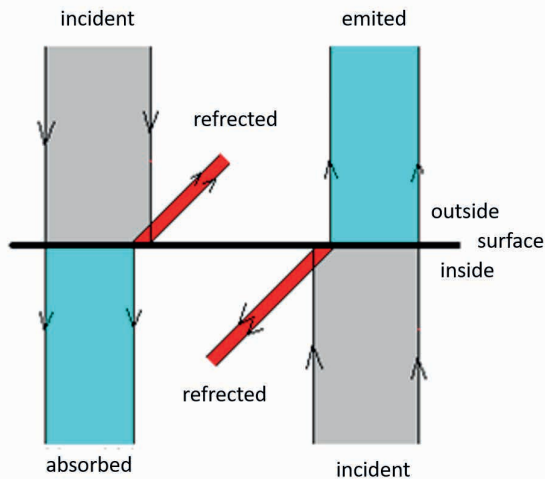


Figure 2. Radiation incident on the surface of a body, where the body absorbs and emits most of the radiation.

Comparing both figures, we observe that a good absorber of radiation is also a good emitter, while a poor absorber is a poor emitter. We can also state that a good reflector is a poor emitter, and a poor reflector is a good emitter. A practical application of this principle can be seen in thermos bottles used to maintain the temperature of liquids such as coffee. A thermos bottle has double glass walls, with a vacuum created in the space between these walls to prevent heat loss through conduction and convection. To reduce radiation losses, the walls are coated with a layer of silver, which is highly reflective, and therefore a poor emitter and absorber of radiation.

2.3 BLACK BODY RADIATION

Blackbody radiation is a fundamental concept in physics that refers to the emission of electromagnetic radiation by an idealized object that absorbs all incident radiation, regardless of wavelength. This object, known as a blackbody, neither reflects nor transmits any radiation, and its emission is solely a function of its temperature. The radiation emitted by a blackbody in thermal equilibrium is characterized by a continuous spectrum, whose intensity and energy distribution depend solely on the body temperature. Planck Law describes this spectral distribution of radiation, demonstrating that the energy emitted at different wavelengths varies with the body temperature, with the peak intensity shifting to shorter wavelengths as the temperature increases, in accordance with Wien's Displacement Law (EISBERG; RESNICK, 1979).

The study of blackbody radiation had significant implications for the development of quantum theory. The discrepancy between classical physics predictions and experimental

results related to blackbody radiation, known as the “ultraviolet catastrophe,” led Max Planck to introduce the quantization of energy. Planck postulated that energy is emitted or absorbed in discrete quantities, called quanta, proportional to the wavelength of the radiation. This hypothesis was crucial for the development of quantum mechanics, as it established the concept that energy is not continuous but quantized. Thus, the theory of blackbody radiation not only elucidated the mechanisms of thermal radiation emission but also laid the foundation for the quantum revolution in physics.

A black body is defined as a medium or substance that absorbs all incident radiation, regardless of wavelength, direction of incidence, or state of polarization. No part of the incident radiation is reflected or transmitted. To understand this concept, imagine a body isolated from its external environment, with insulating walls. As there are no exchanges with the external environment, we say the body is in thermodynamic equilibrium, which means it is in:

- I. *Thermal Equilibrium:* There are no temperature gradients. The temperature of the body is constant and homogeneous.
- II. *Mechanical Equilibrium:* There are no net forces or stresses, meaning the pressure is constant throughout the body.
- III. *Radiative Equilibrium:* The radiation field within the body is constant, meaning the radiation flux entering the body is equal to the flux exiting.
- IV. *Chemical Equilibrium:* The rates of all chemical reactions are balanced by their reverse reactions, so the chemical composition is uniform throughout the body.

Now, suppose this body has a small opening in its wall. All the incident radiation on this opening is absorbed, as the probability of it being reflected back through the same orifice is very low. For this reason, the opening is a perfect absorber or “black”. The radiation that exits through the opening has reached thermal equilibrium with the material constituting the body. This emitted radiation is known as black body radiation and has the following characteristics: it is isotropic, unpolarized, independent of the constitution and shape of the body, and depends only on the body’s temperature and the radiation’s wavelength.

2.4 LAWS OF RADIATION

Wien’s Displacement Law is a fundamental relationship in physics that describes how the spectral distribution of radiation emitted by a blackbody change with temperature. Established by Wilhelm Wien in 1893, this law states that the wavelength at which the emission of radiation from a blackbody is maximal is inversely proportional to its absolute temperature. Mathematically, this is expressed by the formula $\lambda_{\max} = b/T$, where λ_{\max} is the peak wavelength of emission, T is the temperature in Kelvin, and b is Wien’s displacement constant, approximately equal to $2.898 \times 10^{-3} \text{ m}\cdot\text{K}$. This implies that as the temperature of a blackbody increases, the peak of its radiation emission shifts to shorter wavelengths, meaning higher energy regions of the electromagnetic spectrum.

Wien's Displacement Law has important practical and theoretical applications. In astrophysics, for example, it is used to determine the surface temperature of stars by observing the peak wavelength of their emitted radiation. Additionally, this law provides essential insights into the underlying principles of thermal radiation and was a crucial step in the development of the quantum theory of radiation. The observation that blackbody radiation could not be explained by classical physics laws led to the pioneering work of Max Planck, which culminated in the formulation of quantum mechanics. Thus, Wien's Displacement Law not only describes a vital aspect of thermal physics but also played a significant role in the evolution of our understanding of the nature of radiation and energy.

Wien displacement law, is undoubtedly accurate and represents the limit of information achievable through thermodynamic considerations regarding spectral energy distributions. However, it is insufficient to predict the actual shape of an energy spectral curve at any given temperature.

In an attempt to derive a non-failing relationship, Wien made a hypothesis that seemed reasonable at the time: he assumed a certain similarity between a perfect gas and black body radiation, particularly that Maxwell law of molecular velocity distribution for gases would also apply to the radiant energy distribution with respect to frequency for radiation (EISBERG; RESNICK, 1979). The equation he obtained for (R_λ) , the power emitted per unit area and per unit wavelength interval at wavelength (λ) , is given by:

$$R_\lambda = c_1 \lambda^{-5} \frac{1}{e^{c_2/\lambda T}} \quad (1)$$

The Stefan-Boltzmann Law is a fundamental relationship in thermal physics that describes the power radiated per unit area of a blackbody in terms of its temperature. Independently established by Josef Stefan in 1879 and Ludwig Boltzmann in 1884, the law states that the total energy emission of a blackbody is proportional to the fourth power of its absolute temperature. This relationship means that a small increase in the temperature of a blackbody results in a significant increase in the amount of energy radiated.

The Law has wide-ranging applications in various fields of physics and engineering. In astrophysics, for example, it is used to determine the luminosity of stars and other celestial bodies based on their temperatures and radii. Additionally, the law is crucial in the study of heat transfer, where it is applied in the analysis of thermal radiation systems and the design of equipment such as furnaces and heaters. The law also has important implications for understanding energy balances in climate systems and modeling thermodynamic processes. The experimental verification of the Stefan-Boltzmann Law in the 19th century was a major support for the theory of blackbody radiation and helped pave the way for the development of quantum theory.

The Stefan-Boltzmann Law states that the total energy radiated per unit surface area of a black body per unit time (black body radiation), or the energy flux density (radiant flux)

or emissive power, (R), is directly proportional to the fourth power of its thermodynamic temperature (T);

$$R = \sigma T^4 \quad (2)$$

The ultraviolet catastrophe, also called the Rayleigh-Jeans catastrophe, is a failure of classical electromagnetism to explain the electromagnetic emission from a body in thermal equilibrium with its surroundings, or a black body. According to classical electromagnetic predictions, an ideal black body in thermal equilibrium should emit a certain amount of energy at each frequency. When calculating the total energy emitted according to classical theory, it is observed that for longer wavelengths, the classical theory agrees with experimental observations, but for shorter wavelengths, the intensity of emitted radiation tends to infinity, which does not match the experiments. This led to one of the first indications of unresolved problems in classical physics. The solution to this problem led to the development of the first forms of quantum physics, where Planck solved the ultraviolet catastrophe by introducing the concept of discrete energies (RUARK, 1960).

2.5 BASIC CONCEPTS: ABSORPTION AND EMISSION PROCESSES

Between 1854 and 1859, the pioneers of spectroscopy, Bunsen and Kirchhoff, established that although the absorption coefficients (a) and emission coefficients (\mathcal{E}) of a radiating body depend on temperature and its nature, the ratio (a/\mathcal{E}) for a given wavelength depends only on temperature.

For a body in thermal equilibrium with the incident radiation, the ratio between its emissivity E_λ^* and A_λ^* is equal to the spectral radiation density (S_λ^*). Emittance (E_λ^*) is defined as the power radiated per unit area of a radiating surface, and absorptivity (A_λ^*) is defined as the spectral absorbance of the body (DEMTRÖDER, 2010).

$$\frac{E_\nu^*}{A_\nu^*} = S_\nu^*(T) \quad (3)$$

Before Einstein work on the quantum theory of radiation, Max Planck, in October 1906, had formulated an expression describing the behavior of thermal radiation for black bodies. Planck's description originated from adopting statistical methods for studying physical systems, basing his theory on elementary oscillators (radiant atoms) rather than radiation itself. In this work, Planck introduced the concept of discrete energies.

$$\rho_\nu d\nu = \frac{8\pi h \nu^3}{c^3} \frac{d\nu}{e^{h\nu/kT} - 1} \quad (4)$$

Using the relation ($v = c / \lambda$), where the relation between differentials is $dv = - (c / \lambda^2) d\lambda$.

The recording of the black body spectrum is a continuous spectrum.

$$\rho_\lambda d\lambda = \frac{8\pi hc}{\lambda^5} \frac{d\lambda}{e^{\frac{hc}{\lambda kT}} - 1} \quad (5)$$

In 1917, Albert Einstein published the paper “Zum Quantentheorie der Strahlung” (On the Quantum Theory of Radiation) in the journal *Physikalische Zeitschrift*, concerning the relationship between matter and radiation, creating a quantum theory of radiation. In this paper, he based his arguments on statistics and fluctuations. Einstein introduced the concepts of stimulated emission and spontaneous emission (EINSTEIN, 2005).

If an atom or molecule in state (j) with energy (E_j), immersed in a radiation field, is promoted to the excited state (i) with energy (E_i), it must absorb a photon with energy corresponding to the energy difference between the two states: ($h\nu = E_i - E_j$), where h is Planck’s constant and (ν) is the frequency of the absorbed photon. The transition probability between the states is given by equation 2, where (B_{ji}) is Einstein absorption coefficient and $\rho_\nu(\nu)$ is the radiation density, which is the energy per unit volume. The transition probability, dP_{ji}^{abs} , between the states is given by:

$$\frac{dP_{ji}^{abs}}{dt} = B_{ji}\rho_\nu(\nu) \quad (6)$$

where $\rho_\nu(\nu) = n(\nu) h\nu$, and $n(\nu)$ is the number of photons ($h\nu$) per unit volume and within the frequency interval $\Delta\nu = 1\text{ s}^{-1}$. The eq.(6) describes the rate of power absorption of a quantum system from an energy state (i) to an energy state (j) due to interaction with electromagnetic radiation. In this context $\frac{dP_{ji}^{abs}}{dt}$ represents the rate of change of the probability of energy absorption, meaning the frequency at which absorbing transitions occur. The Einstein coefficient for absorption, (B_{ji}), is a constant that characterizes the intrinsic probability of photon absorption for the specific transition between states (i) and (j). Meanwhile, $\rho_\nu(\nu)$ is the spectral energy density of the electromagnetic radiation, indicating the amount of energy present in the radiation field per unit volume and per unit frequency at frequency (ν). Thus, the rate of energy absorption depends on both the intrinsic properties of the quantum system and the intensity of the available radiation at the corresponding frequency, meaning that a higher energy density of the radiation results in a higher absorption rate by the system.

For an atom or molecule in the excited state (E_i), the probability of spontaneous emission to a lower energy state (E_j) is:

$$\frac{dP_{ij}^{em. esp.}}{dt} = A_{ij} \quad (7)$$

where A_{ij} is Einstein coefficient of spontaneous emission.

The probability of stimulated emission is proportional to the energy density, which is the radiation field per unit volume in which the particle is immersed:

$$\frac{dP_{ij}^{em. est.}}{dt} = B_{ij}\rho_v(\nu) \quad (8)$$

where (B_{ij}) is the coefficient of stimulated emission.

Considering (N_i) the number of species (atoms or molecules) in the energy state (E_i) and (N_j) the number in the energy state (E_j) , under steady-state conditions, the emission rate equals the absorption rate, given that (N_i) and (N_j) do not vary with time.

$$B_{ij}\rho_v(\nu)N_j = (B_{ji}\rho_v(\nu) + A_{ji})N_i \quad (9)$$

The eq. (9) represents the dynamic equilibrium between absorption and emission processes in a two-level quantum system. On the left side of the equation, $B_{ij}\rho_v(\nu)N_j$ denotes the rate of photon absorption. This equation encapsulates the balance necessary for thermal equilibrium, where the rate of photon absorption must equal the rate of photon emission. This equilibrium condition is essential for understanding various physical phenomena, including blackbody radiation and the operational principles of lasers and other optoelectronic devices.

In thermal equilibrium, the ratio N_i/N_j is given by the Boltzmann distribution, where g_i is the degeneracy in state (i) and is the degeneracy in state (j) , K is Boltzmann constant.

$$\frac{N_i}{N_j} = \frac{g_i}{g_j} e^{-\frac{(E_i-E_j)}{kT}} = \frac{g_i}{g_j} e^{-\frac{h\nu}{kT}} \quad (10)$$

The eq. (10) describes the population distribution of particles between two energy states (i) and (j) in thermal equilibrium, according to the Boltzmann distribution. Here, (N_i) and (N_j) represent the number of particles in the energy states (i) and (j) , respectively. The term $(E_i - E_j)$ is the energy difference between the states. This expression indicates that the population of particles in a higher energy state (i) relative to a lower energy state (j) decreases exponentially with the energy difference between the states, modulated by the temperature. Additionally, the ratio is influenced by the degeneracy of the states, with higher degeneracy leading to higher population. This relationship is fundamental in understanding phenomena such as thermal radiation and the behavior of gases, and it plays a crucial role in disciplines like statistical mechanics and quantum mechanics (EINSTEIN, 2005).

Explicitly expressing the energy density in terms of the emission and absorption equations for atoms or molecules, we have the following relation. The recording of this radiation is a discrete spectrum.

$$\rho_v(\nu) = \frac{A_{ij}/B_{ij}}{(g_i/g_j)(B_{ij}/B_{ji})(e^{h\nu/kT} - 1)} \quad (11)$$

The expressions by Einstein and Planck both describe the spectral energy density of radiation but from slightly different perspectives, reflecting the historical evolution of our understanding of thermal radiation and the introduction of quantum concepts. Both expressions share a dependence on temperature and use the same exponential form ($e^{h\nu/kT}$) characteristic of the Bose-Einstein distribution for photons, and both include the term ($h\nu$), indicating the quantization of photon energy. However, they differ in their approaches and contexts. Einstein's expression involves specific coefficients and for spontaneous emission, stimulated emission, and absorption, emphasizing the interaction between radiation and a two-level system. In contrast, Planck's expression provides a more direct form, where the spectral energy density depends on the cube of the frequency (ν^3) and universal constants (h) and (c), applying universally to blackbody radiation without specific reference to energy states. Thus, while Einstein's expression offers a detailed microscopic understanding of emission and absorption processes, Planck's expression delivers a macroscopic and universal description of blackbody radiation, making both consistent and complementary in their depiction of thermal radiation behavior. Comparing Einstein's expressions for the discrete radiation emitted by free entities and Planck for the continuous radiation of a black body, we have the following relations:

$$\frac{A_{ij}}{B_{ij}} = \frac{8\pi hc}{\lambda^5} \quad e \quad \frac{g_i B_{ij}}{g_j B_{ji}} = 1 \quad (12)$$

2.6 EMISSION ENERGY

The total energy (E_t) of a molecule in its ground electronic state (excluding translational energy and internal nuclear energy) is given by:

$$E_t = E_e + E_v + E_r \quad (13)$$

where (E_e) is the electronic energy of the ground state, (E_v) is the vibrational energy of the molecule in the ground state, and (E_r) is the rotational energy of the ground state. The vibrational energy (E_v) arises from the periodic motion of the atoms relative to each other within the molecule, while the rotational energy (E_r) results from the rotation of the molecule as a whole around its center of mass. These energy components are fundamental in determining the molecule's overall energy landscape and play crucial roles in various spectroscopic techniques used to study molecular structure and dynamics (HUBER; HERZBERG, 1979).

For the molecule in the excited state, the total energy is given by:

$$E'_t = E'_e + E'_v + E'_r \quad (14)$$

The emission energy of a molecule is the difference in energy between the excited state and the ground state:

$$\Delta E = E'_t - E_t = (E_e + E_v + E_r) - (E'_e + E'_v + E'_r) \quad (15)$$

In spectroscopy, an energy unit commonly used is cm^{-1} . We can write the total energy as follows:

$$T = T_{el} + G(v) + F(J) \quad (16)$$

where $T = \Delta E / hc$, the electronic term is $T_{el} = \Delta E_{el} / hc$, the vibrational term is $G(v)$, $\Delta E_v / hc$ and the rotational term is $F(J) = \Delta E_r / hc$.

A reasonable approximation is to consider that at each moment along the roto-vibrational movement, the spatial electronic distribution instantaneously adjusts to the corresponding nuclear positions, thereby always minimizing the molecular energy. This is known as the Born-Oppenheimer approximation, which allows solving the Schrödinger equation for electronic motion relative to the nuclei of a molecule, considering the latter fixed. One consequence of the Born-Oppenheimer approximation is that the electronic energy is independent of rotational and vibrational energies (HUBER; HERZBERG, 1979).

Vibrational energy originates from the movements of atoms that keep the center of mass of the molecule fixed. We can write the vibrational term more completely as:

$$G(v) = \omega_e \left(v + \frac{1}{2} \right) - \omega_e x_e \left(v + \frac{1}{2} \right)^2 + \omega_e y_e \left(v + \frac{1}{2} \right)^3 \quad (17)$$

where (v) is the vibrational quantum number, (ω_e) is the wavenumber corresponding to the vibration frequency, and (x_e) and (y_e) are the anharmonicity constants, with the index (e) indicating the equilibrium condition.

Rotational energy originates from the rotational motion of the molecule around its axis of symmetry. We can write the rotational term more completely as:

$$F(J) = \widetilde{B}_v J(J+1) + (A - \widetilde{B}_v) \Lambda^2 - \widetilde{D}_v J^2(J+1)^2 \quad (18)$$

where \widetilde{B}_v is the term arising from the rotation-vibration interaction, (J) is the rotational quantum number, (A) is the rotational constant relative to the moment of inertia of the bonding electrons, (Λ) is the projection of the angular momentum along the axis, and is the centrifugal distortion constant as a function of the vibrational state.

Thus, we can write the total energy as follows:

$$T = T_e + \omega_e \left(v + \frac{1}{2} \right) - \omega_e x_e \left(v + \frac{1}{2} \right)^2 + \omega_e y_e \left(v + \frac{1}{2} \right)^3 + \widetilde{B}_v J(J+1) + (A - \widetilde{B}_v) \Lambda^2 - \widetilde{D}_v J^2(J+1)^2 \quad (19)$$

The emission intensity of a spectral line is defined as the energy emitted by a molecule during one second, considering a transition between two states (n) and (m). If there are (N_n) molecules in the initial state and (A_{nm}) is the fraction of molecules in the initial state involved per second in the transition to state (m), this intensity can be expressed by the equation:

$$I_{em}^{nm} = N_n h c \nu_{nm} A_{nm} \quad (20)$$

where $h c \nu_{nm}$ is the energy of each quantum of light with wavenumber ν_{nm} emitted in the transition A_{nm} and is called Einstein transition probability for spontaneous emission.

The intensities of vibronic lines can be estimated based on the Franck-Condon Principle, which states that the mass of the nuclei is much greater than that of the electrons, so the nucleus can be considered static on the timescale of the electronic transition. With the electron in a higher electronic level, the nuclei will react to this new configuration by positioning themselves in a different vibrational state (CARINHANA JUNIOR, 2006). One consequence of the Franck-Condon Principle is that the electronic transition can be described by a vertical line within an energy diagram (Figure 3). The equation below shows the emission intensity:

$$I_{em}^{v'v''} = \frac{64}{3} \pi^4 c N_v \nu^4 \overline{R_e^2} \left[\int \Psi_v' \Psi_v'' dr \right]^2 \quad (21)$$

where N_v is the number of molecules in the upper vibrational state, $\overline{R_e^2}$ is the average value of the electronic transition moment with respect to the internuclear distance, and Ψ_v are the wave functions of the two vibrational states.

Figure 3 shows the quantized potential wells and the corresponding transitions between different vibrational and electronic states of a molecule. The upper potential well represents an excited electronic state, while the lower potential well corresponds to the ground electronic state. Horizontal lines within each well denote quantized vibrational energy levels. Vertical arrows indicate possible transitions between these levels, which can occur either within the same electronic state (vibrational transitions) or between different electronic states (electronic transitions). Absorption of photons can excite the molecule from a lower to a higher vibrational or electronic state, whereas emission occurs when the molecule relaxes to a lower energy state, emitting a photon (HUBER; HERZBERG, 1979).

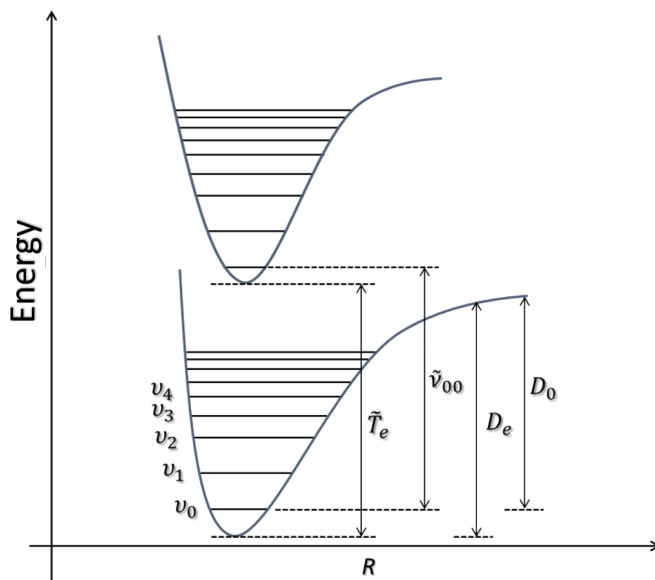


Figure 3. Two potential curves showing the vibrational states associated with each electronic state. The minimum of the upper curve coincides with the minimum of the lower curve.

Figure 4 illustrates the selection rules for rotational transitions within a vibrational-rotational spectrum, highlighting the P, Q, and R branches that correspond to different changes in the rotational quantum number (J) during a vibrational transition. The vertical axes represent the rotational energy levels associated with various vibrational states of a molecule, each labeled with a specific rotational quantum number (J). Red vertical arrows indicate the transitions between these levels, associated with the absorption or emission of photons. The P branch $\Delta J = -1$ corresponds to transitions where the rotational quantum number decreases by one unit, typically appearing on the lower energy side of the spectrum. The Q branch $\Delta J = 0$ involves no change in the rotational quantum number and is less common, occurring mainly in specific vibrational-rotational transitions. The R branch $\Delta J = 1$ represents transitions where the rotational quantum number increases by one unit, usually found on the higher energy side of the spectrum. These selection rules are crucial for interpreting vibrational-rotational spectra, as they provide valuable information about molecular structure, such as moments of inertia and mass distribution (CARINHANA JUNIOR, 2006).

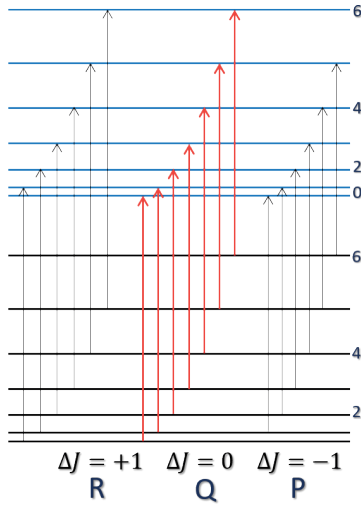


Figure 4. The branch intensities are estimated by the Hönl–London factor for different rotational quantum numbers.

The intensities of rotational or ro-vibrational lines are given by:

$$I_{em} = \frac{2C_{em}v^4}{Q_r} S_J \ln \left(\frac{-B'J'(J'+1)hc}{kT} \right) \quad (22)$$

where C_{em} is an emission constant that depends on the dipole moment variation and the number of molecules in the initial vibrational level, and (S_J) is the line strength, expressed by the Hönl-London factor, representing the intensity distribution along the band, while disregarding possible rotational-electronic interactions (CARINHANA JUNIOR, 2006).

2.7 COMBUSTION

Combustion science can be defined as the science of exothermic processes involving heat transfer and the diffusion of chemical species. This field encompasses a broad range of phenomena, including the detailed chemical reactions that occur during combustion, the thermodynamics of energy release, and the fluid dynamics of reacting flows.

In more detail, combustion science investigates the mechanisms by which fuels ignite, burn, and produce heat and light. This includes studying the kinetics of chemical reactions, the formation of intermediate species, and the pathways leading to the production of combustion products. Researchers in this field also explore the transfer of energy within the system, examining how heat is conducted, convected, and radiated away from the combustion zone.

Furthermore, the diffusion of chemical species is a critical aspect of combustion science. This involves the movement of fuel, oxidizer, and product molecules within the

flame and the surrounding environment. Understanding the diffusion processes helps in predicting flame propagation, stability, and the efficiency of the combustion process.

Advancements in combustion science have significant implications for various applications, including energy production, engine design, and environmental protection. By optimizing combustion processes, scientists aim to improve fuel efficiency, reduce emissions of pollutants, and develop cleaner combustion technologies.

Saturated valence is a concept in chemistry referring to the state in which an atom has all its possible bonds filled with other atoms, achieving a stable electron configuration. In simpler terms, an atom with saturated valence cannot form additional chemical bonds without breaking existing ones.

The definition of fuel and oxidant in the context of combustion is closely related to the concept of saturated valence. A fuel is a substance that can be oxidized, meaning it can lose electrons during a chemical reaction to release energy. Typically, fuels have atoms that are not in their saturated valence state, allowing them to combine with oxygen or another oxidant. Common examples of fuels include hydrocarbons (such as methane, gasoline, and coal), hydrogen, and biofuels. These fuels contain chemical bonds that can be broken to release energy in the form of heat and light.

An oxidant, on the other hand, is a substance that can accept electrons from a fuel during a chemical reaction, facilitating the oxidation of the fuel. Oxidants, like oxygen (O₂), are generally in a saturated or near-saturated valence state but have a high affinity for additional electrons. This characteristic allows them to participate in combustion reactions by accepting electrons from the fuel, thereby enabling the release of energy. Other examples of oxidants include peroxides, chlorates, and some metal oxides.

The formula for the saturated valence of a molecule is:

$$V = \sum_{j=1}^n i_j V_j \quad (23)$$

where i_j is the number of atoms of element j in the molecule, and V_j is the saturated valence of element j . A fuel is a substance whose molecule has a negative saturated valence, meaning $V < 0$. Examples include CH₄, C₃H₈, C₄H₁₀, C₂H₅OH e CH₃OH. An oxidant is a substance whose molecule has a positive saturated valence, meaning ($V > 0$). Examples include O₂, Cl₂ e HNO₃.

A saturated product is formed by molecules resulting from a combustion reaction, where the saturated valence of the molecules is equal to zero, i.e., ($V=0$). Examples include CO₂ and H₂O.

A stoichiometric reaction is a chemical reaction in which the sum of the saturated valences of the reactants equals zero. Consequently, the sum of the saturated valences of the products is also zero.

A mole is defined as the amount of substance that contains 6.022×10^{23} atoms of the isotope carbon-12, which is present in 12 grams of this element. Thus, 1 gram-mole of carbon has a mass of 12 grams.

The molar fraction of species X_i in a mixture of (n) moles is given by:

$$X_i = \frac{n_i}{n} \quad (24)$$

The mass fraction of species (i), with molar mass M_i and number of moles n_i in a mixture, is given by:

$$Y_i = \frac{m_i}{m} = \frac{M_i n_i}{Mn} \quad (25)$$

An equation of state relates the pressure (P), temperature (T), and volume (V) of a gas or a gas mixture. For an ideal gas, intermolecular forces and the volume of molecules are neglected, and the equation of state is given by

$$PV = nR_0 T \quad (26)$$

where R_0 is the universal gas constant ($8.314 \text{ J/mol}\cdot\text{K}$). The total pressure in a gas is equal to the sum of its partial pressures, where the partial pressure (P_i) is given by and the total pressure $P = \sum_i P_i$.

The specific enthalpy (h) of a gas is given by the sum of the specific internal energy (u) and the external energy:

$$h = u + Pv \quad (27)$$

where ($u=U/m$), U is the internal energy.

Specific heats are obtained from the partial derivatives of specific enthalpy with respect to temperature, at constant pressure and volume. Specific heat at constant pressure (c_p) and specific heat at constant volume (c_v) represent the amount of heat required to raise the temperature of a substance by one unit while keeping the pressure and volume constant, respectively.

Specific heat is an intensive property that describes a substance's capacity to store thermal energy. Scientifically, it is the amount of heat needed to raise the temperature of one unit of mass of the substance by one unit of temperature. This concept is crucial for understanding how different materials respond to heat, and it is fundamental in various industrial and scientific processes.

$$c_v = \left(\frac{\partial u}{\partial T} \right)_v \quad \text{and} \quad c_p = \left(\frac{\partial h}{\partial T} \right)_p \quad (28)$$

Enthalpy is a thermodynamic function that represents the sum of the internal energy of a system and the product of pressure and volume. It is a measure of the total energy in a system, including the energy used to perform work against external pressure. Enthalpy is especially useful in processes at constant pressure, such as chemical reactions, where the heat exchanged is directly equal to the change in enthalpy.

$$\bar{u} - \bar{u}_{ref} = \int_{T_{ref}}^T \bar{c}_v dT \quad (29)$$

$$\bar{h} - \bar{h}_{ref} = \int_{T_{ref}}^T \bar{c}_p dT \quad (30)$$

The enthalpy of formation is the heat change that occurs when one mole of a compound is formed from its constituent elements in their standard states at a specified reference temperature, typically 25°C (298 K). This value is crucial for calculating the total enthalpy change in chemical reactions, as it provides a baseline for the energy content of compounds.

Sensitive enthalpy, on the other hand, refers to the change in enthalpy associated with temperature changes in a substance. It indicates how much heat is absorbed or released by one mole of a substance when its temperature changes, without undergoing a phase change. This concept is important for understanding the thermal behavior of substances and is used in various applications, such as heating and cooling processes.

$$\bar{h}_i(T) = \bar{h}_{f,i}^0(T_{ref}) + \Delta\bar{h}_i(T) \quad (31)$$

where $\bar{h}_{f,i}^0(T_{ref})$ is the enthalpy of formation and $\Delta\bar{h}_i(T)$ is the sensitive enthalpy.

Entropy is a measure of the dispersal of energy that occurs in all processes throughout the universe. From a molecular perspective, it corresponds to the occupation of a greater number of energy microstates within a system. The change in entropy is given by $dS = \delta Q/T$, where δQ is the heat exchanged. The specific entropy of formation is:

$$\bar{s}_i(T) = \bar{s}_{f,i}^0 + \int_{T_{ref}}^T \bar{c}_{p,i} \frac{dT}{T} \quad (32)$$

Intensive properties are independent of the mass or volume of a substance. Examples include pressure, temperature, specific enthalpy, and molar specific enthalpy. Extensive properties, on the other hand, are proportional to or dependent on the mass and volume of a substance. Examples include enthalpy, internal energy, and volume.

Viscosity is the proportionality constant between the shear stress (τ) and the velocity gradient (dv/dy) in a flow, expressed as $\tau = -\mu \frac{dv}{dy}$. It is a measure of a fluid's resistance to deformation or flow. In simpler terms, viscosity indicates how "thick" or "sticky" a fluid is, with higher viscosity fluids resisting flow more than lower viscosity fluids.

Viscosity plays a crucial role in combustion processes. It affects the mixing of fuel and oxidant, flame propagation, and heat transfer within the combustion chamber. Higher viscosity can lead to slower mixing and combustion rates, resulting in less efficient burning and potentially higher emissions of pollutants. Conversely, lower viscosity can enhance the mixing and reaction rates, leading to more efficient combustion and cleaner emissions.

The viscosity of a mixture of (N) gases can be calculated using Wilke's semi-empirical expression:

$$\mu_{mixture} = \frac{\sum_{i=1}^N X_i \mu_i}{\sum_{i=1}^N X_j \phi_{ij}} \quad (33)$$

where $\mu_{mixture}$ is the viscosity of the gas mixture, (X_i) is the mole fraction of component, μ_i is the viscosity of component (i), (ϕ_{ij}) is the interaction parameter between components (i) and (j).

The interaction parameter is given by:

$$\phi_{ij} = \frac{1}{\sqrt{8}} \left(1 + \frac{M_i}{M_j} \right)^{-\frac{1}{2}} \left[1 + \left(\frac{\mu_i}{\mu_j} \right)^{\frac{1}{2}} \left(\frac{M_i}{M_j} \right)^{\frac{1}{4}} \right]^2 \quad (34)$$

Thermal conductivity is a constant in the mathematical expression of Fourier's law, $\dot{q} = -k \nabla T$, which relates the heat flux to the temperature gradient. These constant measures a material's ability to conduct heat; substances with low thermal conductivity are thermal insulators, while substances with high thermal conductivity are thermal dissipators.

Thermal conductivity plays a significant role in combustion processes, as it affects heat transfer within the combustion chamber, influencing flame stability, combustion efficiency, and overall energy conversion. High thermal conductivity materials can efficiently transfer heat, promoting uniform temperature distribution and stable combustion, whereas low thermal conductivity materials can hinder heat transfer, leading to localized hotspots and potential combustion inefficiencies.

The thermal conductivity of a mixture of (N) gases can be calculated using the following expression:

$$k_{mixture} = \frac{\sum_{i=1}^N X_i k_i}{\sum_{i=1}^N X_j \phi_{ij}} \quad (35)$$

where ($k_{mixture}$) is the thermal conductivity of the gas mixture.

For polyatomic gases, Eucken developed a semi-empirical formula to calculate thermal conductivity:

$$k = \left(c_p + \frac{5}{4} R \right) \mu \quad (36)$$

Mass diffusivity is a constant in the mathematical expression of Fick's law, which relates the mass flux to the concentration gradient of a species (i) in a mixture: $\dot{m}_i = -D\nabla\rho_i$. When there is a concentration difference in a mixture, the ability of a substance (solute) to disperse in a medium (solvent) is characterized by mass transfer. The diffusion coefficient represents the inverse of the resistance encountered by the solute during this process.

The diffusion coefficient for a binary mixture of gases (A) and (B) can be calculated using the following expression:

$$D_{AB} = 0,0018583 \frac{\sqrt{T^3 \left(\frac{1}{M_A} + \frac{1}{M_B} \right)}}{P \sigma_{AB}^2 \Omega_{D,AB}} \quad (37)$$

where D_{AB} is the diffusion coefficient, σ_{AB}^2 is the collision diameter and $\Omega_{D,AB}$ is the collision integral for diffusion.

Mass diffusivity is crucial in combustion processes as it influences how reactants mix and react. Efficient mixing due to higher diffusivity can lead to more complete combustion, reducing pollutants and increasing energy output. Conversely, low diffusivity can result in incomplete mixing, leading to inefficient combustion and higher emissions. Understanding and calculating mass diffusivity is essential for optimizing various industrial processes, including chemical reactors, combustion engines, and environmental systems, to ensure efficient and effective mass transfer and reaction rates.

The mixture ratio (f), fuel to oxidant by mass, is defined as:

$$f = \frac{m_c}{m_o} \quad (38)$$

where (m_c) is the mass of the fuel and (m_o) is the mass of the oxidant.

The stoichiometric mixture ratio (f_s), fuel to oxidant by mass, is defined as:

$$f_s = \frac{m_{c,s}}{m_{o,s}} \quad (39)$$

where $m_{c,s}$ is the mass of the fuel in a stoichiometric mixture and $m_{o,s}$ is the mass of the oxidant in a stoichiometric mixture.

The equivalence ratio (ϕ) is used to characterize the mixture of fuel and oxidant. It is defined as:

$$\phi = \frac{f}{f_s} = \frac{\frac{m_c}{m_o}}{\frac{m_{c,s}}{m_{o,s}}} \quad (40)$$

For ($\phi < 1$), the mixture is termed as lean, indicating there is more oxidant than needed for complete combustion. For ($\phi = 1$), the mixture is stoichiometric, meaning the fuel and oxidant are present in exact proportions needed for complete combustion. For (> 1), the

mixture is rich, indicating there is more fuel than needed for complete combustion. These ratios are crucial in combustion science as they influence the efficiency and emissions of combustion processes. Lean mixtures tend to produce fewer pollutants but may result in incomplete combustion if too lean. Stoichiometric mixtures are ideal for complete combustion but can produce higher emissions of certain pollutants. Rich mixtures can lead to incomplete combustion and higher emissions of unburned hydrocarbons and carbon monoxide.

A control volume is a fundamental concept in fluid mechanics and thermodynamics used to analyze the behavior of fluids and energy within a defined region in space. It is a fixed or moving region through which fluid can flow in and out, and it is used to apply the conservation laws of mass, momentum, and energy.

In a control volume, the boundaries are defined so that we can focus on the fluid's properties and behavior within that specific region. These boundaries can be real physical surfaces, such as the walls of a container, or imaginary surfaces in an open flow field.

The primary purpose of a control volume is to simplify the analysis of complex systems by isolating a specific region where we can apply the fundamental principles of physics. For example, in analyzing the flow of fluid through a pipe, the control volume might encompass a segment of the pipe, allowing us to study the fluid's properties and changes as it enters and exits that segment.

The First Law of Thermodynamics, also known as the law of energy conservation, states that the total energy of an isolated system is constant, and energy can neither be created nor destroyed, only transferred or converted from one form to another. When applied to a control volume, this law can be expressed in terms of the change in energy within the control volume, the heat added to the control volume, and the work done by the control volume.

For a control volume, the First Law of Thermodynamics can be written as:

$$dE_{mVC} = \delta Q - \delta W \quad (41)$$

where dE_{mVC} is the change in the total energy within the control volume, δQ is the heat added to the control volume and δW is the work done by the control volume.

In this context, the control volume is a defined region in space through which fluid may flow in and out. The energy within the control volume includes internal energy, kinetic energy, and potential energy of the fluid.

The equation signifies that the change in energy within the control volume dE_{mVC} is equal to the heat added to the control volume δQ minus the work done by the control volume δW . Heat δQ represents the energy transfer due to temperature differences, while work δW represents the energy transfer due to force applied over a distance or pressure-volume work.

The adiabatic flame temperature is the temperature of the combustion products when no heat is exchanged with the surroundings and the work done by the fluid in the control volume is zero. This idealized condition assumes that all the energy released during combustion is used to heat the products of the reaction.

The enthalpy of the inflow and outflow in a control volume, considering the First Law of Thermodynamics for an adiabatic flame, is given by:

$$H_e = H_s \quad (42)$$

This can be expressed as:

$$\sum_{j=1}^N n_{e,j} (\bar{h}_{f_{e,j}}^0 + \Delta\bar{h}_{e,j}) = \sum_{j=1}^N n_{s,j} (\bar{h}_{f_{s,j}}^0 + \Delta\bar{h}_{s,j}) \quad (43)$$

where, (H_e) is the total enthalpy of the entering streams, (H_s) is the total enthalpy of the exiting streams, $n_{e,j}$ is the number of moles of component j entering, $n_{s,j}$ is the number of moles of component (j) exiting, $\bar{h}_{f_{e,j}}^0$ is the standard enthalpy of formation at the reference state for the entering streams, $\Delta\bar{h}_{e,j}$ is the sensible enthalpy change for the entering streams, $\bar{h}_{f_{s,j}}^0$ is the standard enthalpy of formation at the reference state for the exiting streams, $\Delta\bar{h}_{s,j}$ is the sensible enthalpy change for the exiting streams.

In an adiabatic process, since no heat is exchanged with the surroundings and no work is performed, the total enthalpy of the reactants must equal the total enthalpy of the products. This concept is critical for calculating the adiabatic flame temperature, which is the highest temperature that can be achieved for given reactants under ideal conditions.

The enthalpy of combustion is the difference between the enthalpy of the products and the enthalpy of the reactants, when the combustion is complete and the products are brought to the same temperature and pressure as the reactants $T_s = T_e$ and $P_s = P_e$ t indicates the amount of heat released by a stoichiometric reaction per 1 kg-mol of fuel. The molar enthalpy of combustion at 298 K and 1 atm, also known as the standard enthalpy of combustion, is given by:

$$\bar{h}_{RP}^0 = Q_{VC} = \sum_{j=1}^N n_{s,j} (\bar{h}_{f_{s,j}}^0) - \sum_{j=1}^N n_{e,j} (\bar{h}_{f_{e,j}}^0) \quad (44)$$

where \bar{h}_{RP}^0 is the standard molar enthalpy of combustion and Q_{VC} is the heat released in the control volume.

The higher heating value (HHV) and lower heating value (LHV) are measures of the energy content of a fuel, representing the amount of heat released during combustion.

The higher heating value (HHV), also known as the gross calorific value (GCV), is the total amount of heat released when a fuel is burned completely, and the products of combustion are cooled to the initial temperature of the reactants, typically 25°C (298 K). This

includes the latent heat of vaporization of the water formed during combustion, meaning that water is in liquid form in the products. The HHV is calculated using the following equation:

$$PCS = - \left[\frac{\bar{h}_{RP}^0}{M_c} \right]_{\text{liquid water}} \quad (45)$$

where M_c is the molar mass of the fuel, the subscript water liquid indicates that the water in the combustion products is in the liquid state.

The lower heating value (LHV), also known as the net calorific value (NCV), is the amount of heat released when a fuel is burned completely, and the products of combustion are not cooled to condense the water vapor formed during combustion. In this case, the water remains in vapor form, and the latent heat of vaporization is not recovered. The LHV is calculated using the following equation:

$$PCI = - \left[\frac{\bar{h}_{RP}^0}{M_c} \right]_{\text{water steam}} \quad (46)$$

The subscript “water vapor” indicates that the water in the combustion products is in the vapor state. These values are critical for determining the energy content of fuels and are used in various applications, such as designing and optimizing combustion systems, calculating fuel efficiency, and comparing different fuels. The HHV is typically higher than the LHV because it includes the energy from condensing the water vapor produced during combustion.

Combustion efficiency is a critical parameter in evaluating the performance of combustion systems, such as engines, furnaces, and boilers. It measures how effectively the chemical energy in a fuel is converted into useful thermal energy during the combustion process. High combustion efficiency indicates that most of the fuel’s energy is being utilized, whereas low efficiency suggests significant energy losses, typically in the form of unburned fuel or heat losses.

Factors influencing combustion efficiency, i) Fuel-Air Ratio: The mixture of fuel and air plays a crucial role in combustion efficiency. The stoichiometric ratio is the ideal proportion where the fuel is completely burned with no excess air. However, in practical applications, slight variations around this ratio are used to optimize efficiency and minimize pollutants. A lean mixture (excess air) can lead to incomplete combustion and higher emissions, while a rich mixture (excess fuel) can cause unburned hydrocarbons and carbon monoxide emissions. ii) Combustion Temperature: Higher combustion temperatures generally improve efficiency by enhancing the reaction rates and ensuring more complete combustion. However, excessively high temperatures can lead to the formation of nitrogen oxides (NO_x), harmful pollutants. iii) Residence Time: The time that fuel and air spend in the combustion chamber affects the completeness of combustion. Sufficient residence time ensures that the reactants have enough time to react fully. iv) Mixing Quality: Proper mixing of fuel and air

ensures a homogeneous mixture, promoting complete combustion. Poor mixing can result in pockets of unburned fuel and inefficiency. v) Heat Losses: Minimizing heat losses to the surroundings can significantly improve combustion efficiency. This includes optimizing the design of combustion chambers and using insulation to reduce heat escape.

Combustion efficiency is typically evaluated using two key metrics:

Thermal Efficiency: This measures the ratio of useful heat output to the total heat input from the fuel. It considers the heat lost in the exhaust gases and other losses but does not account for the completeness of combustion.

Combustion Efficiency: This measures the percentage of fuel that is completely burned during the combustion process. It takes into account the losses due to incomplete combustion (unburned hydrocarbons and carbon monoxide) as well as the thermal losses.

Combustion efficiency (η_c) can be calculated using the following formula:

$$\eta_c = \frac{Q}{PCI} \text{ or } \eta_c = \frac{Q}{PCS} \quad (47)$$

Several strategies can be employed to improve combustion efficiency: **Optimizing fuel-air mixture:** Ensuring the correct stoichiometric ratio for complete combustion. Using advanced burner designs or pre-mixing techniques to ensure a homogeneous fuel-air mixture. **Improving combustion chamber design,** designing chambers to enhance residence time and reduce heat losses. **Regular maintenance,** keeping combustion equipment in good condition to ensure efficient operation, including regular cleaning and tuning of burners.

High combustion efficiency is essential for reducing fuel consumption, lowering operating costs, and minimizing environmental impact by reducing emissions of pollutants. It also improves the overall performance and lifespan of combustion equipment. In industrial applications, optimizing combustion efficiency can lead to significant cost savings and contribute to sustainability goals by reducing greenhouse gas emissions and improving energy utilization.

2.8 FLAME TEMPERATURE

In gases, the concept commonly adopted as temperature corresponds to the average kinetic energy of the particles. However, this concept can only be used in systems in equilibrium. Since a flame does not exhibit thermal equilibrium, the aforementioned definition of temperature cannot be applied to flames (CARINHANA JR. et al., 2008).

In a strictly thermodynamic sense, the concept of temperature can only be applied in an equilibrium state. The term commonly referred to as the “temperature of a system” must be able to describe various properties of a system, including the velocity distribution of all particles according to Maxwell’s equation, the population of excited states according to Boltzmann’s equation, and the distribution of electromagnetic radiation according to Planck’s law. Temperature

must also describe the kinetics of chemical reactions within the system. In systems where these various forms of energy are not in equilibrium, it is useful to adopt a concept of temperature associated with a particular process. Thus, one can assume that the rotational temperature of a species present in a flame is associated with the population distribution of that species along the rotational states belonging to a specific ro-vibrational band. Similarly, the terms vibrational temperature and electronic temperature are used to describe populations of vibrational and electronic levels, respectively (GAYDON; WOLFHARD, 1979).

Investigations into energy transfer processes in systems that do not exhibit thermodynamic equilibrium have shown that in certain cases, the rotational temperature closely approximates the kinetic temperature. This occurs because the translational and rotational energies of the molecules change rapidly according to the conditions imposed on the system. Therefore, determining the rotational temperature from the emission spectrum of radicals present in the flame can be considered a good indicator of the flame's temperature (CARINHANA JR. et al., 2008).

2.9 TEMPERATURE DETERMINATION BY NATURAL EMISSION TECHNIQUE

Conventional methods for determining flame temperatures, such as thermocouples, are limited to temperatures up to about 2000 K. Above this value, the materials currently available undergo oxidation processes that prevent reliable measurements. In such situations, non-intrusive methods, such as spectral analysis of the radiation emitted by the system, have been employed as a viable alternative.

Natural emission spectroscopy is a non-intrusive technique that has the advantage of requiring relatively simple experimental apparatus. Since the species are formed directly in the excited state, a process known as chemiluminescence, it is sufficient to collect the radiation and record the emission spectrum of these species.

In principle, the rotational temperature can be determined from the distribution of the rotational states of any species present in the system. This is commonly done using the method known as Boltzmann Plots, which involves determining the temperature parameter (T) from measurements of the peak intensities (I) of the species' emission spectrum (CARINHANA JR. et al., 2008). The relationship between these quantities can be described by a Boltzmann-type equation, given by:

$$\ln \left(\frac{I\lambda^4}{S_{J'J''}} \right) = \frac{-E_{J'}}{kT} + \ln C \quad (23)$$

where ($S_{J'J''}$) is the Hönl-London factor corresponding to the transition between the upper rotational level (J') and the lower rotational level (J''), which relates to the relative line strengths within a given branch; (C) is a proportionality constant of the same value for all transitions within the same branch. According to this equation, the plot of the natural

logarithm of the intensity term against the energy term is a straight line with a slope whose inverse is the rotational temperature of the species. Therefore, to determine the temperature using this method, it is sufficient to acquire a spectrum with spectral resolution that allows the identification of the rotational lines belonging to a specific vibrational transition.

2.10 EQUIVALENCE RATIO

A typical example of applying emission spectroscopy for temperature determination involves premixed and stationary flames. In this type of flame, two distinct regions are formed, with the lower part of the flame known as the inner cone. The natural emissions of the species C_2^* , CH^* , and OH^* predominantly occur in this region. The other region of the flame is the outer cone, where combustion is partly driven by the oxygen present in the vicinity of the flame.

The temperature of a flame is directly related to the fuel/oxidizer ratio (WARNATZ; MAAS; DIBBLE, 1999). Thus, the stability of a premixed flame depends on the flame's equivalence ratio, given by Equation 24:

$$\phi = \frac{R_{exp}}{R_{est}} \quad (24)$$

where R_{exp} is the experimental fuel/oxidizer ratio and R_{est} is the molar fuel/oxidizer ratio for the stoichiometric reaction. Flames can be classified into rich flames ($\phi > 1$), stoichiometric flames ($\phi = 1$) and lean flames ($\phi < 1$).

2.11 TEMPERATURE DETERMINATION BY THE SODIUM LINE REVERSAL TECHNIQUE

The sodium line reversal (SLR) technique is a simple method that has been widely used for temperature determination in plasmas, solid rocket combustion engines, and hypersonic shock tunnels.

The flame temperature is obtained by comparing the sodium emission spectrum superimposed on the spectrum of an incandescent filament of known temperature, using Planck's radiation law, which relates emission intensity to the system's temperature, according to Equation 25:

$$I_\lambda = \frac{2hc^2}{n^2\lambda^5} \frac{1}{\left[\exp\left(\frac{hc}{n\lambda kT}\right) - 1 \right]} \quad (25)$$

The comparison between emissions is only possible if both have the same solid angle with respect to the detection element. The radiation flux as a function of the solid angle at a given wavelength (Φ_λ) is given by Equation 26, where ε_λ is the emissivity as a function of wavelength, I_λ is the emission intensity, and Ω is the solid angle:

$$\Phi_\lambda = \varepsilon_\lambda I_\lambda \Omega \quad (26)$$

Once the solid angles of the lamp and the flame are adjusted, temperature determination using the sodium line reversal method is based on Kirchhoff's law, which states that a gas in thermodynamic equilibrium has an emissivity (ε) equal to its absorption coefficient (α). The total flux (Φ_{Total}) emitted by the lamp and the flame can be expressed by:

$$\Phi_{Total} = \Phi_{ch}(\lambda, T_{ch}) + (1 - \alpha_{\lambda}) \Phi_{fil}(\lambda, T_{fil}) \quad (27)$$

where Φ_{ch} is the emission flux of the flame and Φ_{fil} is the continuous emission flux of the filament radiation (CARINHANA JUNIOR, 2006).

According to the previous considerations, in the situation where both values are exclusive functions of temperature, the relations between this quantity and the respective values of Φ are expressed in Figure 5 below.

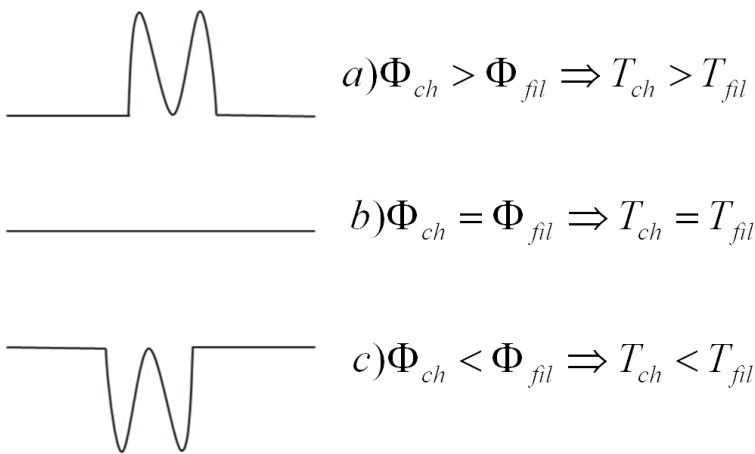


Figure 5. Diagram of the spectra obtained by the line reversal method.

Instead of using the natural emission of excited radicals formed during the combustion process, flames are generally seeded with sodium or iron salts. This procedure serves two purposes: first, to ensure an intense and homogeneous emission throughout the flame, as opposed to radicals, whose distribution is irregular; and second, to provide a narrow atomic emission line, thereby facilitating the comparison process between intensities.

When the flame temperature is higher than the lamp temperature, the emission spectrum of the lamp/flame combination will show an emission peak of the seeding atom superimposed on the continuous emission of the lamp, as illustrated in Figure 5 "a". Conversely, if the lamp temperature is higher, a dip will be observed at the wavelength corresponding to the atomic emission, as shown in item "c". The inversion point, i.e., the threshold where the discrete emission becomes indistinguishable from the continuous emission, corresponds to the situation where both temperatures are equal, as illustrated in item "b". Practically, this is achieved by varying the electric current supplied to the lamp.

METHODOLOGY

3.1 NATURAL EMISSION SPECTROSCOPY

The burner used in the experiment was developed at IEAv. The fuel used was LPG (Liquefied Petroleum Gas), while the oxidizer was O_2 and N_2 was added to the oxidizer to maintain combustion stability. For the calculation of ϕ , the composition of LPG was considered as an equimolar mixture of Propane/Butane. The burner feed was controlled through flow meters calibrated using a primary bubble displacement calibrator, also known as a bubble meter. A total of ten flow meters were calibrated, from which three were selected. The selection was based on their flow ranges that best suited the flows required for the LPG flame configurations.

Various flame compositions were analyzed to select the flames investigated in this work. The basic parameters were the value of ϕ , which ranged from 1.40 to 2.10. Table 1 shows the configurations of the rich flames ($\phi > 1$).

Table 1. Compositions and equivalence ratios of rich flames.

Flame	LPG (mmol/min)	Oxygen (mmol/min)	ϕ
1	7.14	19.6	2.10
2	9.38	52.2	1.33
3	12.1	52.2	1.36
4	14.3	65.8	1.25
5	15.6	59.6	1.51
6	16.1	65.8	1.40

In some mixtures analyzed, issues such as gas flow fluctuations and flow meter instability were observed. These fluctuations caused the flame to detach, making spectrum acquisition unfeasible. In all flames, the nitrogen flow was fixed at 27.0 mmol/min to stabilize the reaction. The flame chosen for study in this work was the one with a burning ratio of $\phi = 1.36$ as it exhibited the greatest stability.

The system used for spectrum acquisition was the Ocean Optics HR 4000 spectrometer. This spectrometer has a fixed grating and a diode array as the radiation detector. Radiation collection is done via a fiber optic cable coupled to the monochromator. A quartz lens is used to focus the flame light into the fiber optic cable. The spectral resolution of this equipment is on the order of 0.16 nm. The experimental setup is depicted in Figure 6.

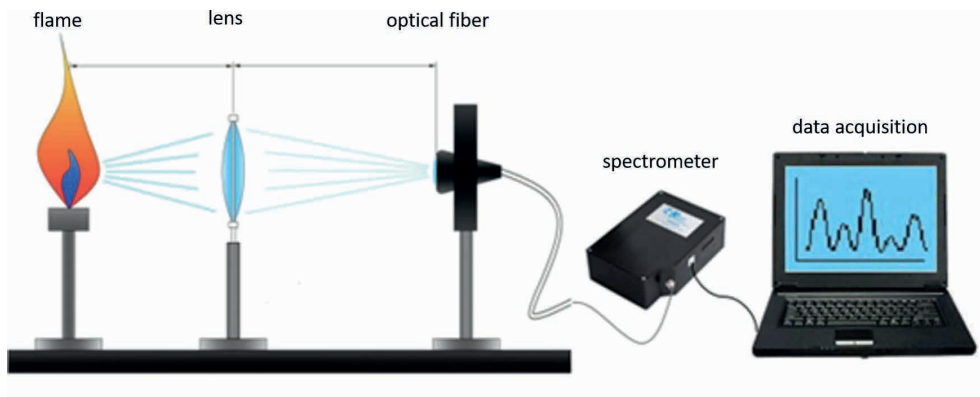


Figure 6. Experimental setup for natural emission

The radical used for mapping was CH^* . Spectra were obtained at eight heights relative to the burner exit, and at each height, nine points were analyzed on the horizontal axis, totaling seventy-two points. A spectrum was recorded at each point, and the flame scanning was performed with a mechanical jack. With the mapping, it was possible to obtain a relative distribution of the CH^* species, whose intensity was obtained from the integral calculation of the spectrum area.

To determine the temperature from the Boltzmann plots, four emission spectra were collected at each preselected point of the flame. This allowed for the determination of the respective standard deviations of the measurements. Temperatures were determined from the emission spectrum of the CH^* radical in the regions of 385 nm and 430 nm, corresponding to the $((\text{B}^2\Sigma-\text{X}^2\Pi))$ and $(\text{A}^2\Delta-\text{X}^2\Pi)$ transitions, respectively. The (A-X) band is observed in the region between 410 and 430 nm. The temperature calculation was based on the analysis of peak intensities located between 418.5 and 423.0 nm. The R1 and R2 branches were investigated, with R1 being the set of peaks of longer wavelength in the doublets. A branch is the set of ro-vibrational lines, originating from transitions of species from higher energy states to lower energy states. According to the characteristics of each of these states, the spectrum presents a specific set of emission lines, called a branch. Each branch line is numbered according to the value of the rotational quantum number of the lower energy level.

In the region from 385 to 410 nm, corresponding to the (B-X) band, there is an overlap of the P and Q branches (FURUYA et al., 1997), preventing the direct application of the Boltzmann equation (Equation 1). To overcome this problem, a second equation was introduced, corresponding to the ratio between the population distribution of the two branches (Equation 28).

$$\frac{I_q}{I_p} = \frac{S_q}{S_p} \exp \left\{ -\frac{hc}{kT_{rot}} [F(N') - F(N' - 5)] \right\} \quad (28)$$

where (I_q) and (I_p) correspond to the experimental measurement of line intensities and (S_q) and (S_p) are the line strengths for the peaks of the Q and P branches, respectively.

The ratio of peak intensities was calculated from an initial estimate of the rotational temperature in Equation 28. Thus, it was possible to construct a system of equations, formed by the sum and the ratio between the emission intensities of each branch. Once the intensities of each line were obtained, the rotational temperature for each branch was calculated. The temperature values obtained were reintroduced into Equation 1 until the best linear fit of the Boltzmann plot was achieved.

Tables 2 and 3 show the parameter values used for calculating the rotational temperature using the Boltzmann plots. R1 and R2 are the branches corresponding to the ro-vibrational lines of the (A-X) band, and RP and RQ are the branches corresponding to the ro-vibrational lines of the (B-X) band.

Table 2. Parameters for temperature determination in the A-X band.

Branch 1				Branch 2			
R1	$S_{j'j''}$	$E'_{rot} (cm^{-1})$	$\lambda(nm)$	R2	$S_{j'j''}$	$E'_{rot} (cm^{-1})$	$\lambda(nm)$
14	9.31	2899.4	422.49	14	8.74	2898.8	422.35
15	9.81	3305.5	421.87	15	9.24	3304.9	421.72
16	10.3	3735.9	421.26	16	9.74	3735.4	421.10
17	10.8	4190.1	420.66	17	10.24	4189.7	420.48
18	11.3	4667.7	420.06	18	10.74	4667.3	419.86
19	11.8	5167.9	419.47	19	11.24	5167.5	419.26
20	12.3	5690.7	418.90	20	11.74	5690.0	418.66
21	12.8	6248.9	418.33	21	12.24	6249.3	418.34
22	13.3	6814.9	417.78	22	12.74	6815.5	417.79

Table 3. Parameters for temperature determination in the B-X band.

Branch P				Branch Q			
RP	$S_{j'j''}$	$E'_{rot} (cm^{-1})$	$\lambda(nm)$	RQ	$S_{j'j''}$	$E'_{rot} (cm^{-1})$	$\lambda(nm)$
6	3.75	26071.8	392.11	11	12.0	27325.0	392.17
7	4.25	26221.5	392.82	12	13.0	27613.4	392.83
8	4.75	26395.4	393.59	13	14.0	27923.2	393.57
9	5.25	26593.2	394.42	14	15.0	28253.5	394.39
10	5.75	26814.3	395.30	15	16.0	28603.7	395.31

3.2 SODIUM LINE REVERSAL

In the SLR experiment, the same burner was used. The gas flow rates used in the flame are shown in Table 4.

Table 4. Burn equivalence ratios and flow meter rates.

Flame (ϕ)	LPG (mmol /min)	O ₂ (mmol /min)
0.97	40	75
1.02	30	50
1.12	55	85
1.36	30	40
1.50	50	65

A 12V DC automotive tungsten filament lamp was used as the light source, with its intensity varied by a high voltage variable DC power supply. Using the optical arrangement shown in Figure 7, the continuous radiation was passed through the flame and recorded by an Ocean Optics compact spectrometer, covering the range from 250 nm to 700 nm. Sodium emission in the burner was produced by inserting small NaCl crystals, resulting in a flame with the appropriate coloration for the technique use. The temperature of the lamp was determined using an optical filament pyrometer.

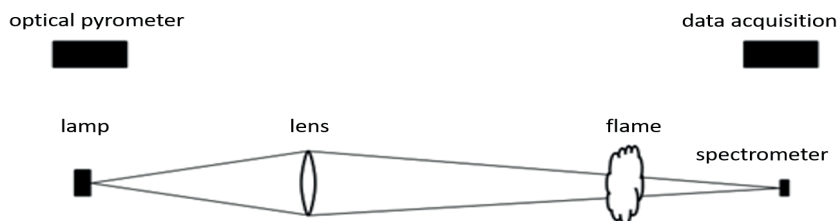


Figure 7. Experimental setup for sodium line reversal

RESULTS AND DISCUSSION

4.1 - RADICAL MAPPING

The presented figure 8 shows the emission spectrum of the CH^{*} radical, characterized by distinct peaks corresponding to electronic transitions between the vibrational and rotational states of the molecule. The (A-X) and (B-X) bands are clearly visible, located in the regions of 410-430 nm and 385-410 nm, respectively. The intensity of the spectral lines provides valuable information about the population distribution of the CH^{*} energy levels, allowing for the construction of Boltzmann plots to determine the rotational temperature of the flame. The spectrum reveals the presence of various rotational branches, such as the R1 and R2 branches in the (A-X) band, as well as the P and Q branches in the (B-X) band, each reflecting specific transitions within the roto-vibrational structure of the radical. This type of spectral analysis is crucial for temperature diagnostics and chemical processes in combustion systems, providing a detailed understanding of the flames internal dynamics and contributing to the development of more efficient and controlled technologies.

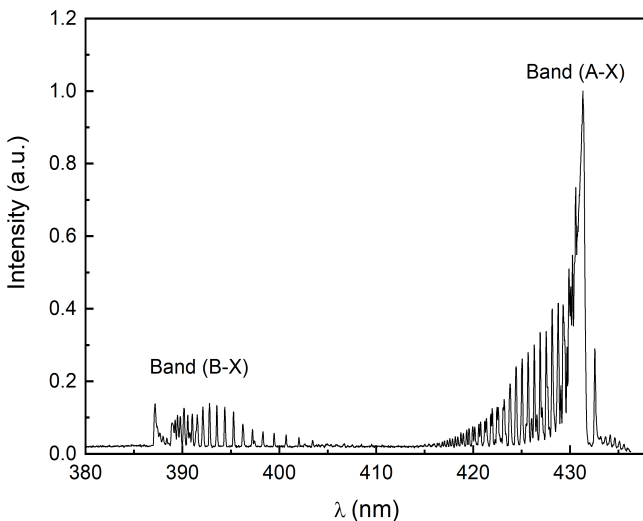


Figure 8. Ro-vibrational spectrum of the CH^{*} radical.

The mapping of the CH* species allowed for the determination of the relative distribution of the CH* species in the investigated flame. Figure 9 shows the variation in emission intensity of the (A-X) band as a function of the height and horizontal plane of the flame. The horizontal axis represents the horizontal plane, where the zero point corresponds to the geometric center of the flame. The legend corresponds to the heights of the flame investigated.

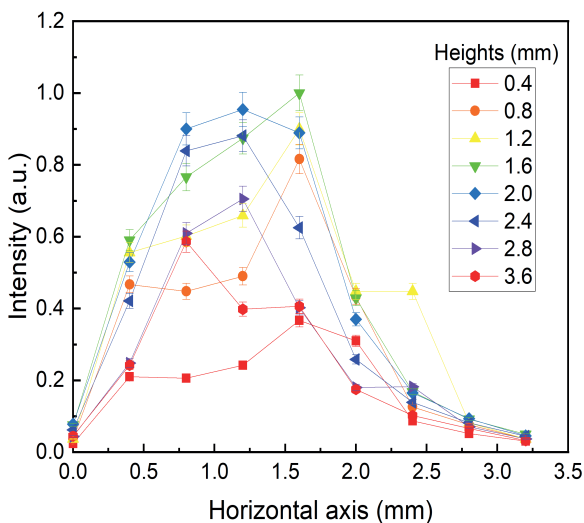


Figure 9. Mapping of the CH* radical in the A-X band of the flame $\phi = 1.36$.

Figure 10 shows the mapping performed from the B-X band of the CH* radical.

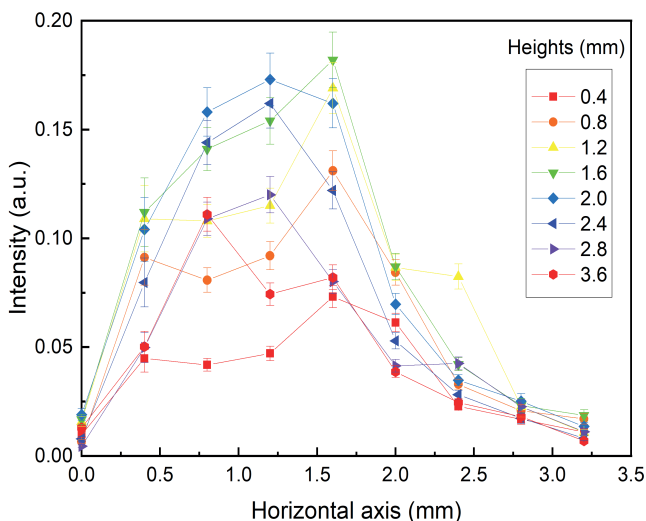


Figure 10. Mapping of the CH* radical in the B-X band of the flame $\phi = 1.36$.

It is observed that the emission signal of the A-X and B-X bands have the same distribution profile, with the A-X band having approximately six times greater emission than the B-X band. The highest emission signal was obtained at a height of 1.2 to 2.0 mm, with the maximum emission intensity in the range of -0.5 to 0 mm on the horizontal axis. From Figures 10 and 11, it can be seen that the distribution of the CH⁺ radical in the flame is not symmetrical. This fact is visually confirmed in the investigated flames and can be attributed to the geometry of the gas exit from the burner's mixing chamber. From the distribution graphs, it was possible to select the regions with the highest emission signal for temperature determination.

4.2 TEMPERATURES CALCULATED USING THE NATURAL EMISSION TECHNIQUE

The points in the flame chosen for temperature determination correspond to the region 1.9 to 3.7 mm above the top of the burner. Their horizontal position was selected based on the highest emission intensity, which corresponds to the region from -0.5 to 0 mm in Figures 10 and 11.

Figure 11 shows the (A-X) band. This band is formed by two branches that are quite far apart, giving rise to a series of doublets. The intensities chosen for temperature determination correspond to peaks 14 to 20.

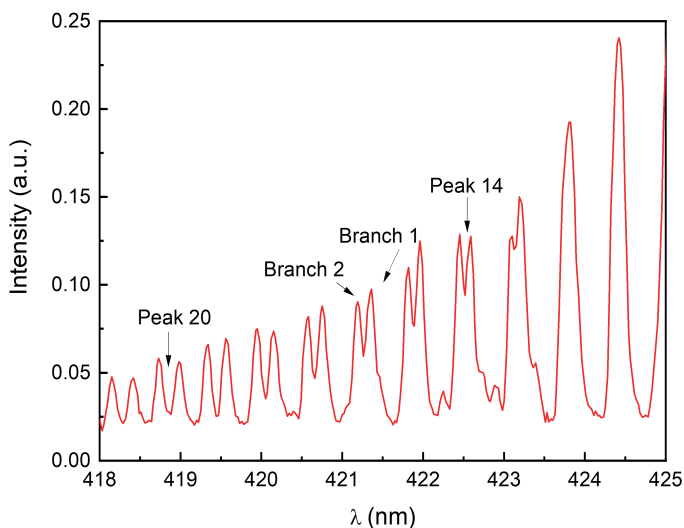


Figure 11. (A-X) band peaks 14 to 20.

For the temperature calculation in the (B-X) band, the P and Q branches were used, which correspond to the peaks P(6) to P(10) and Q(11) to Q(15), as shown in Figure 12. Both sets of P and Q branches have very close wavelengths, so the resulting peak in the spectrum corresponds to the simple sum of the intensities of each line, allowing the application of Equation 28 for temperature estimation.

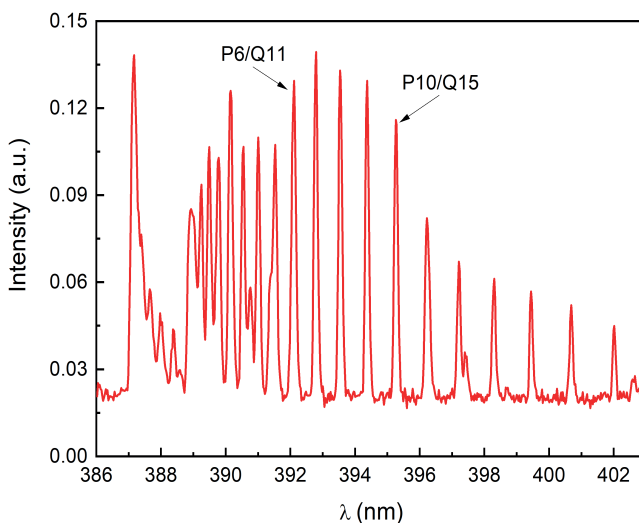


Figure 12. (B-X) band peaks P(6) to P(10) and Q(11) to Q(15).

Figure 13 shows a typical Boltzmann plot of the (B-X) band. Each point corresponds to the experimental intensities, from which the slope of the line is calculated and, consequently, the rotational temperature.

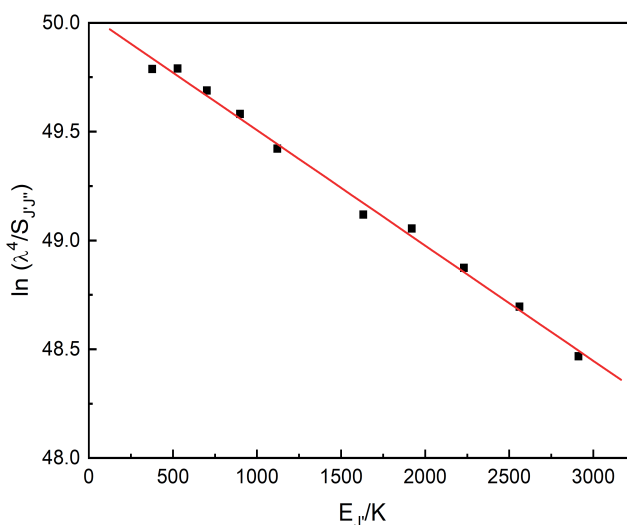


Figure 13. Boltzmann plot of a CH* spectrum, at a height of 1.7 mm above the burner exit and $\phi=1,36$.

The linearity of Figure 14 indicates that the population of the rotational energy states of the CH^{*} radicals follow a Boltzmann distribution. In addition to this observation, it can be inferred that, due to the high coupling between rotational and translational energies, this distribution can be used to characterize the flame temperature.

The rotational temperature values determined for the CH^{*} radical are shown in Table 5. It is observed that the temperature value for R1 in the (A-X) band is lower than that for R2. This result can be explained based on the difference in deactivation rates of the species in the excited state associated with each branch. On the other hand, the temperature values calculated for the (B-X) band are close to the values found in branch 1. In the particular case of the (B-X) band, the method is quite practical, requiring the measurement of the experimental intensity of only five peaks that make up the CH^{*} emission spectrum.

Table 5. Rotational temperatures of the flame $\phi = 1,36$.

Altura (mm)	Temperatura (A-X) R1 (K)	Temperatura (A-X) R2 (K)	Temperatura (B-X) (K)
1.9	2591 ± 51	2746 ± 55	2523±8
2.5	2594 ± 43	2652 ± 13	2571±68
3.1	2526 ± 44	2680 ± 39	2588±44
3.7	2695 ± 56	2894 ± 72	2589±47

4.3 TEMPERATURES CALCULATED USING THE SODIUM LINE REVERSAL TECHNIQUE

Figure 14 shows the black body radiation spectra superimposed on the sodium doublet at wavelengths of 589.0 and 589.6 nm, obtained at different lamp intensities. In Figure 15 “a”, a peak can be observed in the region corresponding to sodium emission, indicating that the flame temperature is higher than that of the lamp, while in Figure 15 “b”, this peak is no longer visible. This condition corresponds to the situation described in Figure 2 (b), where the emission flux of the flame, and consequently its temperature, is equal to that of the lamp. This point is known as the inversion point and is used to determine the flame temperature. As the lamp emission increases, Figure 15 “c”, a sodium absorption peak appears, indicating that in this case, the lamp temperature is higher than that of the flame.

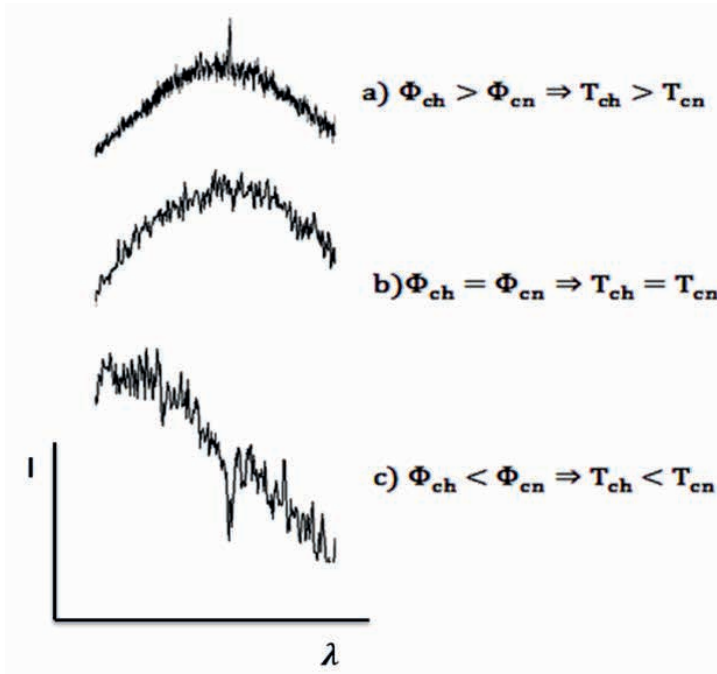


Figure 14. Spectra obtained using the line reversal method: a) sodium emission line; b) inversion point; c) sodium absorption line.

Table 6 shows the burn ratios of the flame, ϕ , the temperature values obtained using the LRS technique, and the adiabatic temperature calculated using the GASEQ program, which represents the maximum calculated temperature for the flame.

Chama (ϕ)	Temperatura (K)	Temperatura Gaseq (K)
0.97	2585 ± 207	3016
1.02	2689 ± 215	2970
1.12	2532 ± 203	3041
1.36	2437 ± 195	2921
1.50	2512 ± 201	2960

Table 6. Flame burn ratios and temperatures (LRS) and GASEQ.

The LRS temperature values are about 15% lower than the adiabatic temperature values, which is consistent with energy dissipation processes in a system like the flame. At the same time, they do not show significant differences when compared to those obtained by spontaneous emission (R1 for the (A-X) band and the (B-X) band), demonstrating the consistency between both techniques. A possible source of measurement error is associated with the amount of sodium present in the flame and the contribution of sodium emission from cooler regions of the flame.

CONCLUSION

The results obtained indicated the feasibility of using the natural emission technique for determining the temperature of combustion systems. The temperature found for branch 1 of the (A-X) band is similar to the temperatures obtained from the (B-X) band, approximately 2500 K to 2700 K. The advantage of employing the Boltzmann plot method lies in the ease of using experimental data to determine the rotational temperature of a species. In the case of the (B-X) band, it requires only the measurement of the experimental intensity of five peaks.

Regarding the sodium line reversal technique, the average temperature values obtained were of the same order as those from branch 1 of the (A-X) band and the (B-X) band. The adiabatic temperature values calculated using the GASEQ program confirmed the consistency of the results obtained. In the future, the natural emission and sodium line reversal techniques could be used to determine the temperature of hypersonic flows in shock tunnels.

BIBLIOGRAPHY

BEDICK, C. R. et al. Combustion plasma electrical conductivity model validation for oxy-fuel MHD applications: Spectroscopic and electrostatic probe studies. **Combustion and Flame**, v. 213, p. 140–155, mar. 2020.

BORKOWSKA-BURNECKA, J. et al. Rotational and vibrational temperatures measured in a chemiluminescent flame from FTIR Bi2 emission spectra. **Journal of Quantitative Spectroscopy and Radiative Transfer**, v. 86, n. 1, p. 87–95, jun. 2004.

CARINHANA JR., D. et al. Determination of liquefied petroleum flame temperatures using emission spectroscopy. **Journal of the Brazilian Chemical Society**, v. 19, n. 7, p. 1326–1335, 2008.

CARINHANA JUNIOR, D. **Determinação de temperatura de chama por espectroscopia de emissão**. Campinas, SP: Universidade Estadual de Campinas, 6 fev. 2006.

DEMTRÖDER, W. **Atoms, Molecules and Photons**. Berlin, Heidelberg: Springer Berlin Heidelberg, 2010.

DIAS, G. S. et al. Experimental study of impinging jets of gelled and liquid fluids. **International Journal of Multiphase Flow**, v. 165, p. 104478, ago. 2023.

DRAKON, A. et al. Soot formation in shock-wave-induced pyrolysis of acetylene and benzene with H₂, O₂, and CH₄ addition. **Combustion and Flame**, v. 198, p. 158–168, dez. 2018.

EINSTEIN, A. Sobre a teoria quântica da radiação. **Revista Brasileira de Ensino de Física**, v. 27, n. 1, p. 93–99, mar. 2005.

EISBERG, R.; RESNICK, R. **Física Quântica, Átomos, Moléculas, Sólidos, Núcleos, e Partículas**. John Wiley & Sons ed. [s.l.: s.n.].

FILGUEIRAS, A. L. C. A. A espectroscopia e a química: da descoberta de novos elementos ao limiar da teoria quântica. **Química nova na escola**, n. 3, p. 22–25, 1996.

FUJISAWA, N. et al. Flickering characteristics and temperature field of premixed methane/air flame under the influence of co-flow. **Energy Conversion and Management**, v. 78, p. 374–385, fev. 2014.

FURUYA, K. et al. Rotational distributions and threshold energies of the CH(B-X) emission by controlled electron impact on methane, ethylene, and ethane. **Chemical Physics**, v. 221, n. 3, p. 303–309, set. 1997.

GAYDON, A. G.; WOLFHARD, H. G. The Spectrum-Line Reversal Method of Measuring Flame Temperature. **Proceedings of the Physical Society. Section A**, v. 65, n. 1, p. 19–24, 1 jan. 1952.

GAYDON, A. G.; WOLFHARD, H. G. **Flames, Their Structure, Radiation, and Temperature**. 4. ed. [s.l.] Chapman & Hall, 1979. v. 1

HUBER, K. P.; HERZBERG, G. **Molecular Spectra and Molecular Structure**. Boston, MA: Springer US, 1979.

- HURLE, I. R.; RUSSO, A. L. Spectrum-Line Reversal Measurements of Free-Electron and Coupled N₂ Vibrational Temperatures in Expansion Flows. **The Journal of Chemical Physics**, v. 43, n. 12, p. 4434–4443, 15 dez. 1965.
- KARABOURNIOTIS, D. Effect of spatial changes in broadening on self-absorbed lines and its impact on plasma diagnostics. **Journal of Physics D: Applied Physics**, v. 40, n. 21, p. 6608–6625, 7 nov. 2007.
- KIM, J. K. et al. LPG, Gasoline, and Diesel Engines for Small Marine Vessels: A Comparative Analysis of Eco-Friendliness and Economic Feasibility. **Energies**, v. 17, n. 2, p. 450, 17 jan. 2024.
- LAGALANTE, A. F. Atomic Emission Spectroscopy: A Tutorial Review. **Applied Spectroscopy Reviews**, v. 34, n. 3, p. 191–207, 27 set. 2004.
- MILES, R. B. Optical diagnostics for high-speed flows. **Progress in Aerospace Sciences**, v. 72, p. 30–36, jan. 2015.
- MOTA, F. A. S. et al. Characterization of the hypergolic ignition of green fuels with hydrogen peroxide by drop test and jet impingement. **Combustion and Flame**, v. 267, p. 113567, set. 2024.
- OSGERBY, I. T.; SMITHSON, H. K.; WAGNER, D. A. Supersonic combustion tests with a double- oblique-shock SCRAMjet in a shock tunnel. **AIAA Journal**, v. 8, n. 9, p. 1703–1705, set. 1970.
- PEJPICHESTAKUL, W. et al. Examination of a soot model in premixed laminar flames at fuel-rich conditions. **Proceedings of the Combustion Institute**, v. 37, n. 1, p. 1013–1021, 2019.
- RUARK, B. O. **Introdução À Física Atômica**. Globo ed. [s.l.: s.n.].
- SIMSEK, S.; USLU, S. Investigation of the impacts of gasoline, biogas and LPG fuels on engine performance and exhaust emissions in different throttle positions on SI engine. **Fuel**, v. 279, p. 118528, nov. 2020.
- SIMURDA, L. J. et al. **Development of a Hybrid Rocket Propulsion System for Small Satellites with Torch Plume Simulation and Temperature Measurements**. United States -- California: [s.n.].
- WARNATZ, J.; MAAS, U.; DIBBLE, R. W. **Combustion**. Berlin, Heidelberg: Springer Berlin Heidelberg, 1999.
- YANG, D. et al. TEMPERATURE MEASUREMENT OF SOLID ROCKET MOTOR EXHAUST PLUME BY ABSORPTION-EMISSION SPECTROSCOPY *. **Spectroscopy Letters**, v. 34, n. 2, p. 109–116, 21 mar. 2001.

DANILO ALMEIDA MACHADO: Is a Brazilian researcher with over 15 years of experience in the aerospace field, specializing in optical diagnostics of fluid flows. He has extensive experience in the development and implementation of optical techniques, including schlieren, shadowgraphy, spectroscopy, laser-induced fluorescence (LIF), particle image velocimetry (PIV), and Rayleigh scattering. His expertise spans studies of multiphase flows, flames, plasma, and shock tunnels. Throughout his career, Danilo has worked on projects involving the development of scramjet engines for hypersonic vehicles, bipropellant rocket engines, and PPT engines for CubeSats. His work has been internationally recognized, earning him prestigious awards such as the Grand Prize at the International Silk Road Symposium on Industry, Education, and Energy Chemical Applications in China, and the Gold Medal in the Edmund Optics Educational Award in the United States. In Brazil, he received the award for the best doctoral thesis in optics from the Brazilian Society of Physics.


Currently, Danilo is a researcher at the Polytechnic School of the University of São Paulo. His previous roles include serving as a professor at the Directorate of Hydrography and Navigation and the Naval College of the Brazilian Navy, and as a research assistant at the Institute of Advanced Studies (IEAv) of the Department of Aerospace Science and Technology (DCTA). Danilo holds a Ph.D. in Space Engineering and Technologies with a focus on Propulsion and Combustion from the National Institute for Space Research (INPE), a Master's degree in Space Sciences and Technologies from the Aeronautics Institute of Technology (ITA), and a Bachelor's degree in Physics from São Paulo State University (UNESP). In addition to his research and teaching, Danilo has published numerous papers in national and international conferences and journals.

Dermeval Carinhana Junior holds a Bachelor's degree in Chemistry, a Master's degree in Chemistry, and a Ph.D. in Chemistry, all from the University of Campinas (UNICAMP), Brazil. He is the Technical Director at the Institute of Advanced Studies (IEAv), where he also served as the Head of the Division of Aerothermodynamics and Hypersonics and the Head of the Postgraduate and Extension Coordination. Additionally, he is a Full Professor in the Postgraduate Program in Aerospace Sciences and Technologies at the Aeronautics Institute of Technology (ITA).

Dermeval is also the Deputy Manager of the Strategic Project "Hypersonic Propulsion 14-X" of the Brazilian Air Force and the Coordinator of the "Flight Test of the Scramjet 14-X S Technology Demonstrator". His research focuses on diagnostic techniques in reactive flows, spectroscopy, and plasma applications. Throughout his career, Dermeval has made significant contributions to the field of aerospace science and technology, particularly in the areas of hypersonic propulsion and advanced diagnostic techniques.

Determination of
Flame Temperature
by Emission and Absorption
Spectroscopy

 www.atenaeditora.com.br


 contato@atenaeditora.com.br


 [@atenaeditora](https://www.instagram.com/atenaeditora)

 www.facebook.com/atenaeditora.com.br

Determination of
Flame Temperature
by Emission and Absorption
Spectroscopy

 www.atenaeditora.com.br

 contato@atenaeditora.com.br

 [@atenaeditora](https://www.instagram.com/atenaeditora)

 www.facebook.com/atenaeditora.com.br